



1 **Atmospheric CO₂ observations and models suggest strong** 2 **carbon uptake by forests in New Zealand**

3 **K. Steinkamp¹, S.E. Mikaloff Fletcher¹, G. Brailsford¹, D. Smale¹, S. Moore¹,**
4 **E.D. Keller², W.T. Baisden², H. Mukai³ and B.B. Stephens⁴**

5 [1]{National Institute of Water and Atmospheric Research, Wellington, New Zealand}

6 [2]{GNS Science, Lower Hutt, New Zealand}

7 [3]{National Institute for Environmental Studies, Tsukuba, Ibaraki, Japan}

8 [4]{National Center for Atmospheric Research, Boulder, Colorado, USA}

9 Correspondence to: K. Steinkamp (kay.steinkamp@gmail.com)

10 **Abstract**

11 A regional atmospheric inversion method has been developed to determine the spatial and
12 temporal distribution of CO₂ sinks and sources across New Zealand for 2011-2013. This
13 approach infers air-sea and air-land CO₂ fluxes from measurement records, using back-
14 trajectory simulations from the Numerical Atmospheric dispersion Modeling Environment
15 (NAME) Lagrangian dispersion model, driven by meteorology from the New Zealand
16 Limited Area Model (NZLAM) weather prediction model. The inversion uses *in situ*
17 measurements from two fixed sites, Baring Head on the southern tip of New Zealand's North
18 Island (41.408°S, 174.871°E) and Lauder from the central South Island (45.038°S,
19 169.684°E), and ship board data from monthly cruises between Japan, New Zealand and
20 Australia. A range of scenarios is used to assess the sensitivity of the inversion method to
21 underlying assumptions, and to ensure robustness of the results. The results indicate a strong
22 seasonal cycle in terrestrial land fluxes from the South Island of New Zealand, especially in
23 western regions covered by indigenous forest, suggesting higher photosynthetic and
24 respiratory activity than is evident in the current *a priori* land process model. On the annual
25 scale, the terrestrial biosphere in New Zealand is estimated to be a net CO₂ sink, removing 98
26 (±37) Tg CO₂ yr⁻¹ from the atmosphere on average during 2011-2013. This sink is much
27 larger than the reported 27 Tg CO₂ yr⁻¹ from the national inventory for the same time period.
28 The difference can be partially reconciled when factors related to forest and agricultural
29 management and exports, fossil fuel emission estimates, hydrologic fluxes, and soil carbon
30 change are considered, but some differences are likely to remain.



1 **1 Introduction**

2 The exchange of carbon between the atmosphere and the earth's oceans and terrestrial
3 biospheres plays a crucial role in climate projections (IPCC, 2013; Friedlingstein et al., 2014).
4 Predicting the future trajectories of atmospheric CO₂, temperature and precipitation requires a
5 solid understanding of how these fluxes are regionally distributed, and how and why they
6 vary on seasonal to decadal timescales. National greenhouse budgets are especially important
7 in light of current policies regarding climate change, such as the annual reporting
8 requirements under the United Nations Framework Convention on Climate Change
9 (UNFCCC).

10 New Zealand's National Inventory Report (NIR) is compiled by the Ministry for the
11 Environment (MfE), and published annually. For 2013, the NIR puts New Zealand's total
12 CO₂ emissions at about 35 Tg CO₂ yr⁻¹, and it is estimated that the land-use and forestry
13 sector acted as a sink for carbon by removing three quarters of that (27 Tg CO₂ yr⁻¹) from the
14 atmosphere (MfE, 2015). These estimates are based on measurements from a network of
15 forest plots throughout New Zealand, regularly updated land use maps, and models. Inventory
16 methods give precise estimates of carbon uptake and release of the locally present vegetation
17 type, but are often difficult to scale up to regional or country scales due to heterogeneous
18 biome composition (Ciais et al., 2010). Independent methods are needed to verify the reported
19 carbon sink.

20 On very large, i.e., continental or global scales, both prognostic land models and inverse
21 atmospheric models have been used (Gurney et al., 2004; Mikaloff Fletcher et al., 2007;
22 Gruber et al., 2009; Le Quéré et al., 2013; Steinkamp and Gruber, 2013; Friedlingstein et al.,
23 2014). Global inversions are a valuable, top-down, tool to estimate large-scale sinks and
24 sources by combining CO₂ observations from a global network with atmospheric circulation
25 models. An inverse model interprets the observations to yield an optimized carbon flux
26 distribution that is most consistent with the atmospheric CO₂ data. In this approach,
27 atmospheric model simulations relate fluxes at the surface with concentration changes at the
28 observing sites. However, the number of available observing sites and the model resolution
29 are usually insufficient to constrain CO₂ exchange on smaller, i.e., regional to country scales.

30 To address those scales, regional atmospheric CO₂ inversions have been developed and used
31 to estimate the carbon budgets of regions like Europe and the USA as well as individual
32 nations (Lin et al., 2003; Stohl et al., 2009; Bergamaschi et al., 2010; Manning et al., 2011). A



1 regional inversion can provide top-down CO₂ exchange estimates from atmospheric CO₂
2 measurements and Lagrangian model simulations that describe the source or sink regions
3 influencing each measurement. They are complementary to bottom-up inventories and
4 provide a means to verify national inventories.

5 Like their global counterparts, regional inversion methods combine CO₂ observations from
6 surface sites with modeled atmospheric circulation to derive the distribution of sinks and
7 sources over an area of Earth's surface (the inversion domain). In a regional inversion,
8 however, the sites are not distributed globally and the domain is typically the size of a country
9 or continent, which poses some additional challenges compared to their global counterparts
10 (Manning, 2011). For example, an accurate model of background concentrations or sinks and
11 sources from outside the inversion domain is required, i.e., a baseline. There is also a need for
12 adequate spatial and temporal resolution for both the estimated fluxes and the circulation
13 model, to account for topographic effects and local emission gradients and hotspots. Many
14 regional inversions use continuous *in situ* observations from one to a few measurement
15 stations to sample the whole domain over the course of days to a few weeks. They use air
16 from a background-sector to construct a baseline time series (Manning et al., 2011; Uglietti et
17 al., 2011). Due to chemical inertness of CO₂, atmospheric loss processes can be neglected
18 once the gas has entered the domain, making this approach viable as long as the measurement
19 station is positioned so that background air can be observed for significant fractions of time. It
20 is generally of advantage to use multiple stations, which are sensitive to a larger surface area
21 and allow for a better interpretation of spatial gradients in atmospheric CO₂.

22 In their inversion study, Stohl et al. (2009) estimate emissions for three HFC and HCFC
23 greenhouse gases on national to global scales for 2005-2007. Their approach uses the
24 FLEXPART Lagrangian model to describe the recent air history arriving at nine observation
25 stations distributed globally. They use *a priori* emission maps and estimate both the baseline
26 and the regional emissions as part of the inverse modeling. Manning et al. (2011) use 20 years
27 of *in situ* CH₄ and N₂O observations from a single station, Mace Head, on the west coast of
28 Ireland. Mace Head regularly receives air from the midlatitude North Atlantic as well as from
29 the UK and continental Europe, which allows them to estimate both the baseline and
30 terrestrial emissions. Their emission estimates for the UK have been used to complement
31 those reported to the UNFCCC for the period 1990-2007.



1 Here, we present the first regional inversion for New Zealand, which leverages the country's
2 unique characteristics. New Zealand is an isolated country surrounded by approximately 2000
3 km of ocean on all sides. This simplifies the construction of an accurate baseline model, as
4 CO₂ signals from other land masses, especially in Australia and the Northern Hemisphere will
5 be significantly diluted and become part of the baseline before reaching the country. The
6 expected national carbon sink, which is estimated by the inversion, is a large fraction of the
7 fossil fuel emissions, which are prescribed – about three quarters according to the NIR. In
8 addition, New Zealand has multiple atmospheric CO₂ measurement sites across a relatively
9 small country.

10 Our inverse model is based on *in situ* observations from two observing stations in New
11 Zealand, between 2011-2013, and ship board measurements from a regular transect between
12 Australia, New Zealand and Japan (conducted by Japan's National Institute for Environmental
13 Studies, NIES). The Numerical Atmospheric dispersion Modeling Environment (NAME III)
14 Lagrangian model (Jones et al., 2007) was combined with meteorological output from the
15 New Zealand Limited Area Model (Davies et al., 2005) at ~12 km resolution (NZLAM-12),
16 to model the pathway of air arriving at the stations. Land model simulations from Biome-
17 BGC (Thornton et al., 2005) are used as *a priori* estimates. We compare our results to New
18 Zealand's NIR (MfE, 2015), point out differences and implications, and discuss the regional
19 distribution and seasonal cycle of CO₂ sinks and sources across the country.

20 **2 Observations**

21 We use *in situ* measurements of CO₂ from two inter-calibrated stations in New Zealand
22 (**Figure 1**). Baring Head (BHD) is located on the south coast of the North Island, while Launder
23 (LAU) is located in the central South Island (**Figure 2**). Both stations are sensitive to different
24 source regions of CO₂ and complement each other to allow for a comprehensive regional
25 coverage spanning the Southern Ocean, Tasman Sea, the South Island, and – to a lesser
26 degree – the North Island and the subtropical South Pacific.

27 The instruments used at LAU and BHD are operated with reference gases traceable to the
28 World Meteorological Organisations mole fraction scale as maintained by the Central
29 Calibration Laboratory (CCL) at the U.S. National Oceanic and Atmospheric Administration
30 (NOAA). Both instruments share common data processing code, improving data inter-
31 comparability between the sites (Brailsford et al., 2012). In addition, fine scale instrumental



1 biases were assessed by using a suite of four transfer standard tanks with trace gas
2 concentrations defined by the CCL. These instrument specific, multiplicative scalings were
3 applied to the processed hourly data before the inversion. For typical ambient mole fractions
4 of CO₂ (i.e. 380-410 ppm) these adjustments were generally less than 0.07 ppm and 0.1 ppm
5 for BHD and LAU, respectively.

6 Some of the elements of this study are prepared to include data from a third station, Rainbow
7 Mountain (RBM), located in the northern half of the North Island (**Figure 2**). For example, the
8 region definitions in section 5.2 include a local RBM region. Because the calibration and
9 quality control processes are equivalent to BHD and LAU, the station can be integrated
10 seamlessly into the network. It is ideally located to extend the sensitivity of the inverse model
11 into the north. However, it is not incorporated in this study, because continuous CO₂
12 measurements from RBM were not yet available through 2011-2013.

13 For this study the hourly mean CO₂ records from BHD and LAU covering 1 January 2011 to
14 31 December 2013 are used. Both stations measure *in situ* with near-continuous observations
15 throughout the day. The observations are strongly influenced by local signals at night and
16 under certain meteorological conditions, e.g., a shallow boundary layer (BL) or low wind
17 speed (Stephens et al., 2013). Measurements at times with deep, well-mixed BL are better
18 suited for inversion modeling as they are sensitive to sinks and sources from a wider region
19 and not subject to localized processes or complex atmospheric structure. Similarly, because
20 the vertical resolution of the meteorological model NZLAM (section 3) is not fine enough to
21 resolve the exact height of a station inlet, conditions with a well-mixed BL are preferable.
22 Afternoon observations are, on average, well-suited. Analysis of the diurnal cycle of CO₂
23 concentrations at the various inlet heights of both BHD and LAU shows least variability with
24 altitude in the 13:00-16:00 afternoon hours. For the inversion, two hourly average data points
25 per day are selected in the afternoon, 13:00-14:00 local time (LT) and 15:00-16:00 LT. Local
26 time represents NZST (NZST = UTC + 12 hours) in winter and NZDT (NZDT = UTC + 13
27 hours) in summer.

28 For both stations, one standard deviation of 5-minute data about the hourly mean is assumed
29 as random data uncertainty. This uncertainty is generally much greater than the measurement
30 imprecision, as it reflects real atmospheric variability, and is instead intended to capture
31 representativeness errors in both the measurement failing to represent the mean of a model
32 box and the model failing to represent the specific conditions at an individual location.



1 2.1 Baring Head

2 BHD station (Lowe et al., 1979) is located at 41.408°S, 174.871°E, 85m AMSL,
3 approximately 10 km southeast of the Wellington urban area (Figure 2), close to the edge of a
4 south facing coastal cliff. The surrounding land is sparsely populated and has primarily been
5 used for low density livestock farming. Wind speeds at the site regularly exceed 10 ms⁻¹,
6 reducing the influence of local sources. The wind directions are primarily bi-modal with the
7 dominant wind from the north and the secondary direction from the south (Stephens et al.,
8 2013). Southerly air arriving at the site has often been traveling over the Southern Ocean for
9 at least 4 days, sometimes weeks, without any contact to terrestrial sinks or sources of CO₂.
10 The station is ideally situated to determine baseline levels of atmospheric CO₂ at latitudes up
11 to 70°S during these conditions. At other times, BHD measures air that has recently travelled
12 over Australia or New Zealand, carrying a terrestrial signal of CO₂ sinks and sources.

13 We use hourly averaged CO₂ data from the non-dispersive infrared (NDIR) analyser
14 (Ultramat 3, Siemens) *in situ* observations during the 13:00-14:00 and 15:00-16:00 time
15 windows (Figure 1) from a 10 m air inlet height. For more details on measurements,
16 calibration and data processing, we refer to Brailsford et al. (2012); Stephens et al. (2013).

17 2.2 Lauder

18 LAU station is located at 45.038°S, 169.684°E, 370m AMSL, in a broad river valley in the
19 South Island, approximately 35 km north of the township of Alexandra (population 5000).
20 The surrounding land is sparsely populated and largely used for low density livestock farming
21 and seasonal cropping. The local wind direction is predominantly ranging from north-westerly
22 to south-westerly. To the west lies a valley system in mountainous terrain, behind which the
23 north-south running mountain range of the Southern Alps divides the island into a western
24 coastal strip with a humid maritime climate and the eastern part with a more continental
25 climate and relatively clear unclouded skies.

26 At LAU, CO₂ has been measured *in situ* using a dual cell NDIR analyser (LI-7000, LI-COR
27 Inc) since 2008 from a 10 m air inlet height. Unlike the BHD measurements, where detailed
28 descriptions and analyses are given by Brailsford et al. (2012) and Stephens et al. (2013), the
29 LAU measurements have not been published before. Therefore, we provide an extended
30 description of the LAU *in situ* CO₂ measurement system in the appendix (Appendix A).



1 **3 Model Simulations**

2 We use NAME III (Jones et al., 2007), a Lagrangian dispersion model developed by the UK
3 Met Office driven by three-dimensional meteorological fields precomputed by a numerical
4 weather prediction (NWP) model. While initially developed more than two decades ago as an
5 emergency response particle tool for nuclear outfall, NAME has since evolved into a general
6 purpose dispersion model that is being used from local scales (a few hundred metres) to
7 mesoscales and global scales. Atmospheric turbulence is simulated using a random walk
8 technique (Morrison and Webster, 2005). CO₂ is modelled as an inert gas due to its long
9 lifetime in the atmosphere far exceeding the 4 day periods used for the back-trajectories.

10 In this work, meteorology from the NZLAM-12 model was used to drive NAME. NZLAM-12
11 is a local configuration of the UK Met Office Unified Model (Davies et al., 2005) with a
12 horizontal resolution of ~12 km and 70 vertical levels up to a ceiling height of 80 km. The
13 meteorology is a sequence of short, 6 hour forecasts with hourly output that are produced
14 from successive NZLAM simulations and cover the period 2011-2013. At the beginning of
15 each simulation the available meteorological observations are assimilated into the model to
16 match the state of the NZLAM atmosphere to the measured atmosphere. NAME uses the
17 boundary layer depth (BLD) from NZLAM and applies a minimum and maximum BLD of 50
18 m and 4000 m, respectively. The maximum height in NAME is 30 km, corresponding to the
19 first 59 levels of NZLAM. Both NZLAM and NAME cover a domain ranging from 146.8 E to
20 185.8 E in longitude and from 53.4 S to 26.0 S in latitude (inversion domain in **Figure 5**).

21 **3.1 Air history and station footprints**

22 The NAME model is run in backward mode to analyse the history of the air traveling towards
23 BHD and LAU over the preceding 4 days. Model particles are released from both stations
24 during a period of 1 hour, twice per day in 2011-2013, at 13:00-14:00 and 15:00-16:00 LT. A
25 simulation period of 4 days was found sufficiently long to allow all particles to leave the
26 domain during most meteorological conditions, except during extended periods of very low
27 windspeed. An air history map has been calculated for each release (**Figure 2**). We use model
28 output that represents the 4-day integrated air concentration (also called dosage, unit g s m⁻³)
29 inside each grid box on a regular 0.1°x 0.1° grid, designed to be very similar to the ~12 km
30 grid of NZLAM-12. During each release, the dispersion of 10,000 particles is modelled and
31 every particle registered within the boundary layer at a given time contributes to the dosage of
32 the respective grid cell. Particles are simulated in 3 dimensions and do not disappear when



1 leaving the boundary layer as long as they remain below the maximum model height of 30
2 km. Particles can leave the boundary layer temporarily and descend back into it at a later time,
3 in which case they would again contribute to the dosage. An example of this can be seen in
4 **Figure 2**, where many particles leave the boundary layer just south of the South Island and
5 later (from the point of view of the backward simulation) descend again, visible as a weaker
6 dosage (less strong colours) for some stretch of the map. A dosage map for a station is also
7 called that station's footprint.

8 Average footprints for the BHD and LAU stations were computed by summing the footprints
9 for every day and release period in 2011-2013 and normalizing them such that the domain
10 integral equals one (**Figure 7**). These footprints represent the average sensitivity of a station to
11 spatially distributed surface fluxes (sinks and sources) of CO₂. They have also been used to
12 help inform the partitioning of the inversion domain into a set of regions for which weekly
13 surface fluxes are calculated (Section 5.2).

14 **3.2 Transport matrix**

15 For particle transport, the mass flux during each 1 h release period is 1 g CO₂ s⁻¹, amounting
16 to a total emission of 3600 g CO₂ over the period (0.36 g CO₂ is assigned to each particle).
17 The flux strength is an arbitrary choice and does not affect the transport results due to the
18 implied linearity of transport. A transport matrix T (unit s m⁻¹) is formed by dividing the
19 dosage by the total emitted mass and multiplying by the area (m²) of each surface grid cell.
20 Each element of T describes the atmospheric transport of a continuous emission of 1 g CO₂
21 m⁻² s⁻¹ from a given grid cell over the previous 4 days and subsequent contribution to the air
22 concentration at the receptor (BHD or LAU) during each 1 h period. With \mathbf{x} being a vector
23 containing all grid cells and \mathbf{c} a vector containing the concentration (unit g CO₂ m⁻³) for all 1
24 h periods, this is written as

$$25 \quad T\mathbf{x} = \mathbf{c} \quad (1)$$

26 Given T and the measured concentrations \mathbf{c} , the inversion developed in this work solves for
27 the CO₂ fluxes \mathbf{x} using a Bayesian optimisation, i.e., a statistical model that balances
28 information from measurements with *a priori* knowledge about the fluxes (section 6). Instead
29 of solving on the grid scale, the fluxes in \mathbf{x} are pre-aggregated into a set of regions and *a*
30 *priori* flux maps are taken into account for the terrestrial and oceanic portions of the domain
31 (section 4).



1 **4 A Priori CO₂ Flux Maps**

2 The Bayesian approach in this study uses spatially distributed information about CO₂ sinks
3 and sources as first-guess, or *a priori*, fluxes for terrestrial and oceanic regions. These fluxes
4 are optimized by the inversion using the constraints imposed by the CO₂ measurements at the
5 stations (section 6). Fossil emissions are accounted for as well, though unlike the natural
6 fluxes they are prescribed and not optimized by the inversion. Here we describe the data sets
7 and flux maps used, while their incorporation in the inversion is described in section 5.

8 **4.1 Terrestrial**

9 First-guess land-to-air CO₂ fluxes from the biosphere for every month in 2011-2013 are
10 obtained from the Biome-BGC model (Thornton et al., 2005). Biome-BGC (v4.2 final
11 release) is an ecosystem process model that estimates the storage and flux of carbon, nitrogen
12 and water (Thornton et al., 2002). The model has been extensively tested and validated for
13 North American and European ecosystems, and in addition was recently extended and applied
14 to New Zealand managed pasture systems (Keller et al., 2014). The adaptation of the Biome-
15 BGC model to New Zealand by Keller et al. (2014) is used in this study to estimate net
16 ecosystem production (NEP) for 5 biomes across New Zealand: dairy pasture, sheep and beef
17 pasture, shrub, evergreen broadleaf forest (EBF), and evergreen needleleaf forest (ENF). The
18 model is driven by daily weather data from the NIWA virtual climate station network
19 (VCSN). VCSN data include numerous meteorological parameters on a regular (~5 km) grid
20 covering the whole of New Zealand (Tait et al., 2006). The data are based on the spatial
21 interpolation of actual data observations made at climate stations located around the country.
22 Soil attributes are incorporated from the Fundamental Soil Layers database (Landcare, 2015).

23 Biome-BGC produces NEP maps for each biome covering the whole country, i.e., it does not
24 make assumptions about the actual distribution of biomes. In order to partition the country
25 into biomes approximating the five categories available in Biome-BGC and then mask and
26 sum the NEP contributions from each biome, we produced a land-cover/land-use (LCLU)
27 map. The LCLU map uses 10 categories based on a combination of the land cover database
28 (LCDB) for New Zealand (Shepherd and Newsome, 2009; Dymond et al., 2012) and the
29 Land-Use in Rural New Zealand (LURNZ) model (Hendy et al., 2007; Timar, 2011; Kerr et
30 al., 2012).

31 The New Zealand LCDB is a thematic classification of land-cover and land-use categories,
32 created using satellite imagery and covering all of mainland New Zealand. Version 3 was



1 used here, which contains 33 categories for each of three periods; summer 1996/97, summer
2 2001/02, and summer 2008/09. The dataset is polygon-based and designed to be compatible
3 in scale and accuracy with Land Information New Zealand's 1:50,000 topographic database.
4 For the purpose of this study the distribution of land-cover types for 2008/09 were used and
5 rasterized on a 5 km x 5 km grid.

6 LURNZ is a dynamic partial equilibrium model that simulates changes in private rural land
7 use over time and space. It focuses on four key land uses – dairy, sheep and beef, forestry
8 (plantations), and scrub/shrubland. While the model's primary focus is on simulating future
9 changes in land-use under scenario projections of commodity prices in one of the four sectors,
10 it also provides a baseline of actual land-use in 2008. This 2008 basemap is used in this study
11 to match the Biome-BGC dairy and sheep/beef pasture biomes; however, LURNZ does not
12 include native forests.

13 To account for all biomes in Biome-BGC the LURNZ 2008 basemap and the LCDB 2008/9
14 land-cover map are combined as follows. First the 33 LCDB categories are aggregated into 7
15 – forest, scrub and shrubland, grassland, cropland, water bodies, bare or lightly-vegetated
16 surfaces, and artificial surfaces. The forest and grassland categories are then sub-divided into
17 plantations, “other forests”, dairy pasture, sheep and beef pasture, and “other grasslands”
18 using LURNZ, which results in the LCLU map in **Figure 3a**.

19 The ENF biome is assumed to be well represented by the plantation forest category, with
20 plantations consisting primarily of pine trees. The EBF biome is assumed to be better
21 represented by the “other forests” category. The categories of artificial surfaces, bare/lightly-
22 vegetated surfaces, and water bodies are assigned a zero flux, i.e., no exchange of CO₂ with
23 the atmosphere. No flux estimates are made for cropland and “other grasslands”; this does not
24 affect results significantly, because these categories represent only a small portion of the total
25 land area. **Figure 3b** shows the 2011-2013 mean *a priori* land-to-air CO₂ flux as estimated by
26 matching the LCLU and Biome-BGC biomes in this manner and summing their contributions
27 to the overall NEP. The monthly and annual contributions are shown in **Figure 3c**. Weekly
28 first-guess CO₂ flux maps are obtained by simple interpolation of the monthly estimates
29 throughout 2011-2013.

30 An uncertainty estimate is computed for the *a priori* CO₂ flux from each grid cell. Based on
31 Keller et al. (2014) and personal communication with the authors, we assign a 10%
32 uncertainty for pasture land. For forests, we assign 10% everywhere except in the Canterbury



1 and Otago regions in the South Island, where 56% and 36% are used, respectively. These are
2 conservative estimates based on a comparison of the Biome-BGC modelled live stem carbon
3 with the national exotic forest regional yield tables (MPI, 2012). The Canterbury and Otago
4 regions were assigned larger uncertainties to reflect the larger discrepancy between the
5 Biome-BGC model and the yields in these regions. The uncertainty is taken into account by
6 the Bayesian optimization (Section 5).

7 **4.2 Oceanic**

8 First-guess air-sea CO₂ fluxes are calculated based on a global dataset of surface ocean pCO₂
9 (Takahashi et al., 2009a). The dataset contains approximately 4.5 million measurements of
10 surface water partial pressure of CO₂ (pCO₂) obtained over the global oceans during 1968-
11 2008, approximately 90,000 of which were taken inside the model domain of this study. A
12 monthly climatology on a global 4x5 grid was derived by Takahashi et al. (2009b), which also
13 includes an estimate of air-sea CO₂ flux derived from the difference of surface ocean and
14 atmospheric CO₂ and a gas exchange rate following Wanninkhof (1992).

15 An uncertainty estimate for the *a priori* ocean fluxes is computed as the root mean square of
16 two components reflecting the uncertain gas exchange rate and the spatiotemporal coverage of
17 measurements inside grid cells. For the first component we recalculated the CO₂ flux using
18 each of 7 additional gas transfer models (Ho et al., 2006; Sweeney et al., 2007) and used one
19 standard deviation from the 8-model mean as uncertainty. The second component applies an
20 uncertainty to grid scale fluxes inversely proportional to the number of measurements taken
21 inside them for a given month of the climatology (Steinkamp and Gruber, 2013). As with the
22 terrestrial CO₂ flux prior, the uncertainty is accounted for in the Bayesian inversion.

23 **4.3 Fossil emissions**

24 A gridded map of CO₂ emissions is derived from the Emission Database for Global
25 Atmospheric Research (EDGAR) version 4.2 (JRC, 2011). EDGAR contains global emission
26 inventories for greenhouse gases and air pollutants from sectors including energy, industrial
27 processes, solvents and other product use, agriculture, land-use change and forestry, and
28 waste. Annual emissions are available on a 0.1°x0.1° grid over the globe up to the year 2010.
29 Emissions for the 2011-2013 time period were approximated by extrapolation using the trend
30 in global total emissions over 2000-2010. The spatial distribution was assumed unchanged
31 from 2010 (Figure 4). Total emissions for the New Zealand mainland are 47.8 Tg CO₂ yr⁻¹ in
32 2011-2013.



1 Fossil CO₂ emissions are not optimized by the inversion, but their contribution to the CO₂
2 signal at both stations (**Figure 8**) is subtracted from the actual measurements beforehand. That
3 contribution is calculated using the transport matrix from NAME, i.e., applying Equation (1)
4 with \mathbf{x} containing the emissions from every grid cell and week in 2011-13. The vector \mathbf{c} then
5 contains CO₂ concentrations for the twice-daily release periods at both stations that are caused
6 by the emissions. To convert concentrations into mole fractions (ppm) the atmospheric
7 pressure and temperature from the NAME model are used, which were interpolated to the
8 BHD and LAU site coordinates from the NZLAM-12 temperature and pressure fields.

9 **5 Regional Flux Estimation**

10 **5.1 Baseline analysis**

11 Any regional CO₂ inversion can only estimate sinks and sources within the boundaries of the
12 model domain. Sink and source processes from outside the domain become part of the CO₂
13 background concentrations (i.e., baseline) seen by the regional inversion at the boundary.
14 Therefore, an accurate description of this baseline is needed. A common approach is the
15 background-sector method (Manning et al., 2011; Uglietti et al., 2011), where air is classified
16 as baseline if it originates from a certain wind sector and fulfils site specific meteorological
17 criteria. A continuous baseline is constructed using gap-filling, which is subtracted from all
18 other measurements before the inversion. The inverse model then interprets these differences,
19 or anomalies, to find the optimal distribution of sinks and sources within the model domain.

20 The background-sector method has been applied to the BHD CO₂ record by Brailsford et al.
21 (2012) and Stephens et al. (2013). They use steady background CO₂ mole fractions during
22 southerly wind conditions at BHD and apply a multi-step filter to the BHD record to obtain a
23 CO₂ baseline representative of a large region over the Southern Ocean. In short, the filter
24 selects measurements during extended periods of southerly winds at the site, during which a
25 maximum standard deviation of 0.1 ppm is achieved. Additional meteorological conditions
26 must be fulfilled to preclude the influence of local sources and to ensure the air has not passed
27 over the South Island before arriving at BHD. After filtering the data for baseline conditions,
28 a continuous baseline is constructed using the seasonal time series decomposition by Loess
29 (STL) algorithm (Cleveland et al., 1990), which can be sampled hourly, i.e., during the 13:00-
30 14:00 and 15:00-16:00 LT release periods. The baseline derived from the BHD record is
31 shown in red in **Figure 1** and will be called the southern baseline.



1 One disadvantage of a background-sector approach based on a single site is that it may not
2 capture variability in background concentrations from different wind conditions, in particular
3 along the latitudinal axis with its gradient in atmospheric CO₂, which could lead to biases in
4 the flux estimates within the domain. In our case, BHD's background sector is ideally situated
5 to obtain a CO₂ baseline representative of a large region over the Southern Ocean. However,
6 observations made during northerly events are not always well described using this baseline,
7 as the air often originates from the northern Tasman Sea or the subtropical South Pacific and
8 carries a contribution from Northern Hemisphere CO₂ (Section 6, **Figure 7**).

9 To alleviate this we augment the southern baseline with a second baseline from ship data
10 representative of the northern sector. This northern baseline is based on *in situ* CO₂
11 observations using a NDIR analyser on board the Trans Future 5 (TF5), a ship of opportunity
12 that cruised the triangle Japan/Australia/New Zealand about once a month during the period
13 2011-2013 (Chierici et al., 2006). We mask out data points from along the ship track (**Figure 5**)
14 to keep observations from the open ocean and avoid observations taken close to the land,
15 especially near the Australian east coast as it is located upwind during average south-westerly
16 conditions and hosts large urban centres with significant CO₂ emissions. These data are then
17 latitudinally averaged between 26-27°S to produce a baseline representative of the northern
18 edge (26°S) of the inversion domain. A continuous baseline is constructed using the same
19 STL routine as for the southern baseline.

20 For both baselines, uncertainty estimates are formed based on the monthly standard deviations
21 of the *in situ* data as well as differences between measurements and the STL smoothed curve.
22 A more detailed description of the construction of both baselines is provided in the appendix
23 (Appendix B).

24 A combined CO₂ baseline is constructed that takes into account where the modelled
25 trajectories originated for any given data point. The daily NAME station footprints for the
26 13:00-14:00 and 15:00-16:00 LT windows are integrated along the southern and northern
27 edges of the domain to determine the relative fraction of back-trajectories leaving the domain
28 to the south and north. These fractions are then used to weigh the two baselines and create a
29 baseline associated with each of the twice-daily data points. Uncertainties are weighed in the
30 same way. The combined baseline is shown in green in **Figure 1**. For the plot the 13:00-14:00
31 and 15:00-16:00 LT weighted baselines were averaged, as they are visually almost
32 indistinguishable, but the individual baselines are used in the inversion.



1 **5.2 Regional partitioning**

2 CO₂ fluxes are estimated for every week in 2011-2013 and for 25 geographic regions
3 distributed across the inversion domain (**Figure 6**). The within-region pattern of the fluxes is
4 prescribed using the *a priori* flux maps for New Zealand and the surrounding oceans, while
5 the inversion estimates regional totals. The definition of the regional boundaries was guided
6 by several factors, including the distance from the measurement stations, the gradient of the
7 station footprint, local orography, and fossil emission hotspots. For land regions in New
8 Zealand, additional factors include land-cover and land-use types as well as the expected
9 (first-guess) CO₂ flux distribution.

10 Due to its large distance from the stations, the portion of Australian land inside the inversion
11 domain is represented by a single region (#16). No *a priori* information about natural CO₂
12 fluxes from Australia is assumed, i.e., they are set to zero with a very large uncertainty of
13 1000 Tg CO₂ yr⁻¹, so that the inversion is free to adjust them. This is based on an analysis
14 showing generally low sensitivity of CO₂ measurements at our stations in New Zealand to
15 Australian fluxes (Section 6, **Figure 8**). The analysis uses fossil emissions from the Australian
16 region (section 4.3) and investigates whether these emissions leave a significant imprint on
17 measured CO₂ at BHD and LAU. Except for a few days this imprint is negligible (section 6).

18 The portions of the Southern Ocean, South Pacific and Tasman Sea that are inside the model
19 domain were divided into 6 open ocean and 3 coastal regions (#17-25). The open ocean
20 regions are large to make their regionally integrated contribution to the CO₂ signal become
21 discernible at the stations, though still much smaller compared to the land regions in New
22 Zealand. They divide the domain into three northern and three southern regions to account for
23 the difference in ocean biogeochemistry between Southern Ocean and subtropical Pacific
24 waters, with guidance from patterns of surface ocean pCO₂ from the *a priori* map. The coastal
25 ocean regions were included to separate the open ocean from the land explicitly, and to
26 account for their stronger influence on the measured CO₂ due to their relative proximity to the
27 stations compared to the open ocean. The coastal ocean was defined as the union of a 60 km
28 coastal band around New Zealand and the portion of ocean with a mean 2011-2013 BHD
29 footprint value above a fixed threshold. The threshold was chosen such that the integrated
30 CO₂ signal at BHD from coastal regions is 25% of that from all ocean areas.

31 It is generally important to separate regions that exhibit a strong variability in sensitivity, as
32 otherwise these within-region gradients can skew the regional totals estimated by the



1 inversion towards the most sensitive areas inside the region. For land regions in New Zealand,
2 we used the spatial gradients of the 2011-2013 footprints as an estimate for this variability,
3 similar to the coastal regions, except that for the land, we use the combined footprint of BHD
4 and LAU (Figure 9) and also account for additional factors.

5 New Zealand was divided into 15 land regions (#1-15) as follows. Three small regions around
6 BHD, LAU and RBM were defined, which have the largest contributions to the CO₂ signal at
7 the respective stations. This separation of the highly influential local regions from the rest of
8 the country follows the same rationale as the separation of the coastal from the open ocean,
9 with the aim to prevent the inversion from allocating local signals to regions further upwind.
10 A separate region around Auckland and Hamilton was defined to capture the strong fossil
11 emissions there. The remaining regions were defined with the aim to minimize both the
12 footprint variability and the expected flux variability inside each region, while accounting for
13 topographic features and avoiding many different types of land-cover/land-use in the same
14 region.

15 The resulting regional partitioning is shown in Figure 6. A major feature is the role of the
16 Southern Alps as a dividing range between the humid west coast of the South island
17 containing large patches of native forest, and the dryer regions in the central and eastern parts,
18 where pasture land is predominant. On the North Island, the axial mountain ranges divide the
19 land into east and west as well, but the distribution of forests and pasture is more complex.
20 BHD and LAU have relatively low sensitivity to the northern half of the North Island, which
21 results in large uncertainties after the inversion for individual regions. However, regionally
22 aggregated results are well constrained in that part of the country.

23 5.3 Inversion methodology

24 The aim of the inverse method is to estimate a CO₂ flux from every region and for every week
25 between 2011 and 2013 using a Bayesian approach (Gurney et al., 2004; Tarantola, 2005;
26 Steinkamp and Gruber, 2013). The approach assimilates information from the twice-daily
27 observations from both stations (the “data”) and accounts for *a priori* flux distributions (the
28 “prior”) and contributions from fossil emissions.

29 The data time series is constructed by subtracting the baseline from the station measurements.
30 The modelled CO₂ signal from fossil emissions is also subtracted. The resulting time series
31 represents the part of the observed CO₂ signal that cannot be explained by background
32 concentrations or fossil emissions, but is due to the net effect of sinks and sources of CO₂



1 over the ocean and land portions inside the model domain. The data for every 1 h period and
 2 both stations is written as a vector \mathbf{d} .

3 Data uncertainty is calculated as the quadrature sum of the baseline uncertainty (Section 5.1)
 4 and the CO₂ data uncertainty (Section 2). An additional uncertainty component of 0.4 ppm is
 5 assumed to account for uncertainties in the inverse modeling system as well as possible errors
 6 in the fossil fuel emission estimates. That value is based on a goodness of fit analysis of the
 7 inverse model (reduced chi-squared statistic, as described below). The final data uncertainty is
 8 taken as the root mean square (quadrature) of both components. The square of the uncertainty
 9 populates the main diagonal of the data covariance matrix C_d . We assume no correlations
 10 between pairs of data points, so all off-diagonal elements of C_d are set to zero.

11 The regional prior (denoted \mathbf{x}_0) is obtained by integrating the weekly *a priori* terrestrial and
 12 oceanic flux maps over each of the 24 non-Australian regions. The prior uncertainty is
 13 similarly obtained by aggregating the grid-scale uncertainty estimates. Since the within-region
 14 flux patterns remain fixed, we assume full spatial correlation when propagating grid-scale
 15 uncertainties to the regional scale. For land regions we added (via root mean square) an
 16 additional uncertainty component of 50% of the seasonal flux amplitude. This is to allow the
 17 inversion to shift the seasonal cycle more freely; without it the seasonal turning points – i.e.
 18 the switch between net CO₂ uptake in the summer months and net release in the winter –
 19 would essentially be fixed as the flux is near zero and the grid-scale uncertainty estimates for
 20 the Biome-BGC model are proportional to the flux strength. The diagonal prior covariance
 21 matrix C_0 contains the regional uncertainty.

22 The regional prior is linked to the data vector as in Equation (1), except \mathbf{x} now contains fluxes
 23 on the regional instead of grid scale, and the transport matrix T links regional total fluxes to
 24 the data time series with baseline and fossil signal subtracted.

25 The inversion process seeks an optimal solution to the transport equation by balancing the
 26 data and prior constraints (Tarantola, 2005), i.e., by minimizing a Bayesian cost function J
 27 with respect to \mathbf{x} ,

$$\begin{aligned}
 J &= \frac{1}{2}(\mathbf{T}\mathbf{x} - \mathbf{d})^T C_d^{-1}(\mathbf{T}\mathbf{x} - \mathbf{d}) + \frac{1}{2}(\mathbf{x} - \mathbf{x}_0)^T C_0^{-1}(\mathbf{x} - \mathbf{x}_0) + \frac{1}{2}(\mathbf{S}\mathbf{x})^T C_s^{-1}(\mathbf{S}\mathbf{x}) \\
 28 \quad &= \frac{1}{2}(\tilde{\mathbf{T}}\mathbf{x} - \tilde{\mathbf{d}})^T \tilde{C}_d^{-1}(\tilde{\mathbf{T}}\mathbf{x} - \tilde{\mathbf{d}}) + \frac{1}{2}(\mathbf{x} - \mathbf{x}_0)^T C_0^{-1}(\mathbf{x} - \mathbf{x}_0)
 \end{aligned}
 \tag{2}$$



1 The first term in the equation evaluates the deviation of the modelled time series from the
 2 data, with each data point weighted with the inverse uncertainty. The second term evaluates
 3 the deviation of the optimized regional fluxes to the prior fluxes. The last term is a Gaussian
 4 smoother being used to limit changes in week-to-week fluxes. The operator S forms a vector
 5 whose elements correspond to the difference of each flux in \mathbf{x} and the flux of the following
 6 week. The diagonal matrix C_s contains values representing the strength of the smoother. We
 7 chose $5 \text{ kg CO}_2 \text{ m}^{-2} \text{ yr}^{-1}$ for every grid cell, translating into slightly different values on the
 8 regional scale due to varying surface areas. This value is more than ten times larger than the
 9 largest flux from any grid cell of the *a priori* flux maps (Figure 3), hence the smoother is very
 10 weak. In fact the smoother was designed to have a negligible effect on estimated CO_2 fluxes
 11 and not interfere with the prior and data constraints. Its role is merely to favour solutions with
 12 small week-to-week changes in cases where a second solution with much larger week-to-
 13 week changes would result in a very similar cost, J . Due to their mathematical forms being
 14 equivalent, the smoothing term can be absorbed in the data term in Equation (2) by appending
 15 S to T (forming \tilde{T}), C_s to C_d (forming \tilde{C}_d), and a zero vector of appropriate length to \mathbf{d}
 16 (forming $\tilde{\mathbf{d}}$). The reduced chi-squared statistic $\chi^2 = 2J/n$ is used to assess the fit of the
 17 inverse model to the observations (Gurney et al., 2004; Baker et al., 2006). The number of
 18 degrees of freedom, i.e. the number of observations minus the number of sources, is denoted
 19 by n . Inclusion of the aforementioned data uncertainty component of 0.4 ppm ensures $\chi^2 \approx 1$,
 20 which means that the extent of the match between observations and the model as well as
 21 between the *a priori* and *a posteriori* sources are in accord with their respective uncertainties.
 22 The cost function in Equation (2) is minimized analytically (Enting, 2002; Tarantola, 2005),
 23 to yield *a posteriori* fluxes \mathbf{x} and covariance matrix C ,

$$\begin{aligned}
 \mathbf{x} &= C(\tilde{T}^T \tilde{C}_d^{-1} \tilde{\mathbf{d}} + C_0^{-1} \mathbf{x}_0) \\
 C &= (\tilde{T}^T \tilde{C}_d^{-1} \tilde{T} + C_0^{-1})^{-1}
 \end{aligned}
 \tag{3}$$

24 The square root of the diagonal elements of C are reported as uncertainty estimates for the *a*
 25 *posteriori* fluxes.

26

27 5.4 Sensitivity scenarios

28 Considerable effort has been undertaken to ensure, e.g., the high quality of available
 29 observations, the inter-comparability of measurements from BHD and LAU, and the use of a



1 state-of-the-art land process model to provide meaningful first-guess estimates. However,
2 there are a number of potential sources for bias that cannot be accounted for explicitly, but
3 could have a significant influence on estimated land fluxes. These include (i) the CO₂
4 baseline, (ii) the modeling in NAME, and (iii) the ocean prior fluxes.

5 Sensitivity scenarios were designed to address each of these potential biases, as described
6 below. The results are discussed in section 7.4.

7 (i) The inverse method assumes that air entering the domain is accurately characterized by the
8 baseline CO₂ time series. While random noise in the baseline concentration is accounted for
9 (Section 5.1), there remains the possibility of systematic bias. A positive (negative) bias in the
10 baseline would cause the inversion to estimate a total CO₂ flux that is depressed (elevated), in
11 order to explain the measurements at the stations. It is assumed that this effect is most
12 pronounced at the edge of the domain, i.e., in the Australian and open ocean regions. To
13 address its significance to the inner regions, sensitivity runs were conducted with both
14 positive and negative biases. The baseline mixing ratio is first decreased, then increased, by
15 one standard deviation, i.e., its uncertainty.

16 (ii) The CO₂ fluxes are assumed constant in time over a one week period and their geographic
17 distribution within each region is fixed. A CO₂ flux pulse lasting only a few hours cannot be
18 resolved and could bias the weekly average flux if it coincides with a high sensitivity during
19 the pulse. Otherwise, its contribution will be correctly contained in the weekly average flux,
20 unless the region is being unevenly sampled. That is, if a specific observation is sensitive to
21 only a small area inside the region, then the flux estimate for the entire region will be biased
22 towards that area, which may not be representative for the region. This is why we took the
23 geographic distribution of biomes into account when defining the regions. The number of
24 different biomes was minimized and isolated patches of biomes avoided inside each region.
25 However, the region definition remained subjective, so we included a sensitivity case where
26 the within-region flux pattern is flat, i.e., the flux is constant region-wide. Not all potential
27 biases are removed this way, as that would require solving the inverse problem at a much
28 higher resolution, but it gives an indication of the influence of a particular choice of pattern.

29 (iii) Estimates of terrestrial CO₂ fluxes in New Zealand are influenced by the ocean flux prior
30 through atmospheric transport. After entering the model domain at baseline levels, the air
31 travels inevitably over a large stretch of ocean and will arrive at the New Zealand coast
32 carrying an oceanic signal in its CO₂ concentration and the difference to the measurements at



1 the stations will be interpreted by the inversion in terms of terrestrial CO₂ flux. In a sensitivity
2 test, we excluded the ocean prior to isolate its impact on the results.

3 **6 Analysis of New Zealand's *in situ* CO₂ Observing Sites**

4 We conducted a clustering analysis using NAME III to characterise the catchment areas of the
5 BHD and LAU stations. The clustering was performed using a convergent k-means
6 procedure, which is based on Kidson (1994), but adjusted slightly to allow a larger number of
7 trajectories to be clustered, i.e., by using a smaller number of random seeds. This significantly
8 boosts the computation at the expense of likelihood to find the global minimum, however, the
9 reduced number of seeds appeared large enough to come sufficiently close, as repeated
10 computations with randomly different subsets all produced very similar results.

11 A set of 1000 trajectories was used between 15:00-16:00 LT for every day in 2011-2013,
12 resulting in approximately 1 million trajectories for each station. The number of clusters was
13 set to 7, because this number maximised the distinctness of clusters with respect to each other
14 as obtained from their silhouette values. Cluster centroids and sizes are overlain on the station
15 footprints in **Figure 7**, together with the geographical width of the clusters.

16 In addition to the clustering analysis, we applied Equation (1) to the *a priori* flux maps for
17 every day in 2011-2013. This allows us to calculate the imprint of Australian and New
18 Zealand fossil emissions as well as oceanic and New Zealand terrestrial sinks and sources on
19 the CO₂ concentration measured at BHD and LAU (**Figure 8**).

20 CO₂ measurements at BHD are most sensitive to sinks and sources in the Southern Ocean
21 (south of 55°S), the Tasman Sea and the South Island. Australia and the North Island
22 influence BHD CO₂ to a lesser extent. Observations at LAU are strongly influenced by local
23 to regional terrestrial sinks and sources of CO₂, enabling the station to see air from a large
24 portion of the southern South Island.

25 The low sensitivity to Australia means it is infeasible to infer Australian CO₂ fluxes with our
26 observational network most of the time. On the other hand, this underscores the isolation of
27 New Zealand, where air is received that largely contains background concentrations from the
28 vast body of surrounding ocean. This allows us to estimate terrestrial fluxes in New Zealand
29 with high sensitivity and little disturbing influence from continental sources.



1 **6.1 Baring Head**

2 In 2011-2013, BHD sampled air that has travelled from the Southern Ocean 41% of the time
3 along two cluster pathways (**Figure 7**), which correspond to southerly wind conditions at the
4 site. The more southerly cluster of the two (16%) contains trajectories that mostly have not
5 seen land over at least 4 days and will carry Southern Ocean baseline CO₂. Trajectories in the
6 more westerly cluster (25%) have travelled across most of the South Island after originating in
7 the Southern Ocean and will carry a signal of the terrestrial sinks and sources of CO₂ there.
8 Another 17% of trajectories are originating from the south-west, but are associated with
9 slower wind speeds, so that within the 4-day timeframe of the back-trajectories they have not
10 yet left the domain. They correspond to a local northerly wind at BHD associated with a
11 common synoptic pattern involving an anticyclone over the Tasman Sea. The Southern Alps
12 on the South Island strongly influence the south-westerly air flow and deflect it northward
13 along the west coast and then through Cook Strait, where it is channelled into a northerly flow
14 by local topography. Trajectories arriving from Australia and the Tasman Sea occur 13% and
15 9% of the time, respectively. 10% of the trajectories have crossed large parts of North Island
16 before arriving at the station.

17 The application of Equation (1) to the *a priori* flux maps shows that there are only 4 days in
18 2011-2013 when a discernible (larger than 0.1 ppm) signal from Australian fossil fuel
19 emissions within the inversion domain was received at BHD. The signal was always smaller
20 than 0.4 ppm, the minimum overall uncertainty assumed in the modeling system.

21 During the winter and summer seasons New Zealand land is the main contributor to the BHD
22 data series, with a seasonal pattern matching the respiration and growing cycles. Assumed
23 aseasonal fossil emissions from New Zealand (mostly from the nearby city of Wellington) as
24 well as seasonal oceanic fluxes also play an important role at BHD.

25 **6.2 Lauder**

26 For LAU, there are two southwest clusters representing a combined 40% percent of
27 trajectories. These are very similar in size to the corresponding clusters for BHD, and have
28 identical source areas in the Southern Ocean. Both clusters differ in whether the air flow leads
29 to local winds at LAU from the west or south. While similar to BHD's southern cluster, the
30 air from the southern cluster would have travelled over a considerable stretch of land before
31 arriving at LAU. 14% of the time, the air being sampled belongs to another southwestern
32 cluster, which originates in the Tasman Sea. In addition, there is a western cluster containing



1 15% of trajectories that has crossed South Australia and the Tasman Sea as well as two
2 northern clusters representing air with mixed origin from the northern Tasman Sea or the
3 North Island. About 14% of trajectories are contained in a slow cluster whose origin is not
4 very far from LAU. These cases correspond to slow winds at the site and indicate that the
5 measurements are highly impacted by local and regional sources as the air has been travelling
6 over nearby land for the preceding 4 days.

7 The application of Equation (1) to the *a priori* flux maps shows that LAU station is dominated
8 by terrestrial fluxes from New Zealand (particularly from South Island), with only minor
9 contributions from the ocean, reflecting its location further inland and shielded from the
10 predominant westerly winds by the Southern Alps. The seasonal amplitude in the CO₂ signal
11 at LAU is about twice as large as at BHD, due to the more continental climate and more
12 pronounced growing seasons in central South Island. Similar to BHD, there are only 5 days in
13 2011-2013 when a larger than 0.1 ppm signal from Australian fossil fuel emissions within the
14 inversion domain was received at LAU.

15 **7 Flux Results and Discussion**

16 **7.1 Seasonal cycle**

17 The inversion finds a much stronger seasonal cycle than the Biome-BGC model simulations
18 used as a prior (**Figure 3c**), especially associated with enhanced CO₂ uptake during the
19 growing season in (austral) summer (**Figure 10**). There is very good agreement in the phasing
20 of the seasons with the land process model during all 3 years, which is particularly
21 encouraging in light of the weak constraints on the phasing applied through the prior (section
22 5.3). This strong seasonality is robust within the estimated *a posteriori* uncertainty range and
23 across the sensitivity cases. Uncertainties for weekly fluxes were reduced significantly
24 compared to the prior, even when the range of sensitivity cases is added as extra uncertainty.

25 The enhanced seasonal amplitude is assigned to the South Island almost exclusively, with
26 much stronger uptake during the growing season compared with carbon uptake in Biome-
27 BGC. The uncertainties associated with South Island fluxes are generally smaller than on the
28 country scale, because of the high sensitivity of the LAU and BHD stations to fluxes from
29 much of the South Island. On the other hand, the North Island is estimated to have a weaker
30 seasonal cycle, in good agreement with the prior, which can be attributed to widespread areas
31 of summer soil water deficits, and the more marine climate there, i.e., weaker seasonal



1 temperature variations and milder winters. Uncertainties for North Island fluxes, especially
2 from the northern half of the North Island, are generally larger due to the lower sensitivity of
3 the stations to that area. While northerly breezes are very common at BHD (**Figure 7**), they
4 often correspond to a situation where southwesterly air was deflected by the Southern Alps
5 and channelled by local topography to turn into a northerly at the station. Air that has
6 travelled across the North Island and picked up its terrestrial CO₂ signal is therefore less often
7 sampled at BHD than local wind direction would suggest. At LAU, North Island air can be
8 sampled only about 8% of the time, based on the NAME cluster analysis. In a future study,
9 the sensitivity to North Island fluxes can be greatly enhanced by CO₂ observations at the
10 recently established RBM station in central North Island.

11 When separating the South Island into parts east and west of the Southern Alps, it becomes
12 apparent that most of the enhanced seasonal cycle occurs, in fact, in the west, despite the
13 slightly smaller surface area (86,173 km² compared to 88,348 km²). Along the west coast, the
14 inversion estimates the seasonal amplitude to be more than twice as large as suggested by the
15 prior. Tracing the cause further to the individual regions reveals that Fiordland (region #13) is
16 the strongest contributor to the signal. Fiordland is extremely sparsely populated and covered
17 to a large extent by indigenous temperate rainforest with southern beeches, fern trees and
18 shrub. When forming the prior flux map, these forests were categorized as evergreen
19 broadleaf forest (EBF) and the respective module from Biome-BGC used. However, the EBF
20 module had not been optimized for New Zealand forests, so it is possible that the Fiordland
21 forests are not well described by that category. The inversion suggests much stronger
22 photosynthetic and respiratory activity in these forests than the prior model.

23 **7.2 Response to the 2012/2013 drought**

24 The austral summer of 2013 was characterised by unusually high temperatures and low
25 precipitation over much of New Zealand (Turner, 2013; Blunden and Arndt, 2014), with
26 sustained periods of severe drought in February-March 2013. The North Island and the west
27 of the South Island were the most strongly affected regions (Porteous and Mullan, 2013). The
28 Biome-BGC model is driven by detailed, reanalyzed weather data and clearly shows a
29 positive flux anomaly, i.e., loss of CO₂ to the atmosphere, due to enhanced respiration and
30 inhibited growth during that period (**Figure 3e**). The inversion sees this event in the
31 observations as well, suggesting even more CO₂ release than Biome-BGC across the South
32 Island. Unfortunately, a prolonged data gap in the LAU time series during that period caused



1 by a lack of field standards (**Figure 1**), leads to weaker constraints from the atmospheric CO₂
2 data and therefore larger uncertainty in the flux estimates in the South Island.

3 A signal of excess CO₂ release in February-March 2013 is seen by the inversion across the
4 North Island, too (**Figure 10**). The limited coverage of some areas in the North Island,
5 especially in the north and east (**Figure 9**), leads to high annual mean flux uncertainty for
6 individual regions and prevents a robust analysis as to which regions responded the most
7 strongly to the drought. Eddy covariance data from a dairy pasture site in the northwestern
8 North Island during a ~100 day drought in 2008 found a temporary loss of CO₂ to the
9 atmosphere, but the ecosystem recovered to become a net sink of CO₂ for the year (Mudge et
10 al., 2011).

11 **7.3 Annual fluxes**

12 The geographic air-land flux distribution averaged over 2011-2013 is shown in **Figure 11**,
13 including flux gradients on the sub-regional level that were prescribed in the inversion. A
14 comparison to the *a priori* distribution in **Figure 3b** shows larger areas acting as a net carbon
15 source. These include the central and north-eastern parts of the South Island, which roughly
16 correspond to the Canterbury region and mostly contain pasture land, in particular sheep and
17 beef pasture (**Figure 3a**). The inversion does not, however, resolve ecosystem processes, but
18 merely estimates net air-land fluxes, so it is not possible to make a link between pasture and a
19 net CO₂ source. A counterexample is the south-east of the South Island, which also contains
20 large areas of pasture, but is estimated to be a net carbon sink. In general, the inversion
21 assigns much more of the total land sink to forested areas than the Biome-BGC prior. This is
22 particularly apparent along the western South Island, but also in the eastern half of the North
23 Island. The strong flux gradients seen in region #3 are likely to be the result of the very
24 heterogeneous composition of LCLU types there, combined with BHD and LAU having low
25 sensitivity in the region (**Figure 9**), rather than a real signal. The inclusion of an additional
26 station with high sensitivity to the northern North Island, such as RBM, would be needed to
27 improve flux estimates there.

28 In the inset of **Figure 11**, we compare annual mean results from the inversion with bottom-up
29 estimates from the National Inventory Report (MfE, 2015), or NIR. The inversion suggests a
30 much larger net CO₂ sink across the country compared to the NIR. Particularly in the forest of
31 the south-western South Island, the inversion suggests both stronger photosynthetic and
32 respiratory activity than the prior model, with the overall balance towards a larger CO₂ sink



1 over the course of a year. For example, Fiordland appears to take up between 22 and 68 Tg
2 CO₂ each year in 2011-2013 (Table 1), which corresponds to per-area uptake rates of 614 and
3 1899 g CO₂ m⁻² yr⁻¹, respectively. By comparison, the Biome-BGC estimates range from 0 to
4 3 Tg CO₂.

5 The NIR estimates do not come with an overall uncertainty, but based on their reporting of
6 typical uncertainty for individual ecosystems, and personal communication, an approximate
7 figure of 50% was identified. This implies statistical significance for the difference in annual
8 sink estimates, except in 2013, when both estimates agree within their uncertainty range.
9 Without ocean prior or by assuming a baseline bias of 0.1 ppm, the differences are reduced by
10 up to a half (section 7.4), but do not disappear. How can these differences be explained?
11 There are a number of possible scenarios, which we explore in the following.

12 The accounting of fossil emissions differs between the NIR and the inversion. The EDGAR
13 emissions of 47.8 Tg CO₂ yr⁻¹ prescribed in the inversion contain elements of land-use change
14 and agriculture, which will therefore not be part of the posterior flux estimates. The NIR gives
15 total emissions of 34.6 Tg CO₂ yr⁻¹ for 2013. The difference of about 13 Tg CO₂ yr⁻¹ would
16 appear in the inversion as an additional sink of equal size.

17 The inversion and NIR estimates are not directly comparable, due to differences in the top-
18 down versus bottom-up viewpoints. While the inversion sees the overall net CO₂ exchange
19 between the atmosphere and the land, the NIR estimate represents the so-called LULUCF
20 sector, i.e., it includes contributions from Land-Use, Land-Use-Change and Forestry. In the
21 LULUCF model, it is assumed that CO₂ emissions from harvested wood products occur at the
22 location of the tree, a process particularly important to forest plantations located in the central
23 North Island and in the north of the South Island (Figure 3a). However, about 70% of the
24 biomass from forest harvesting is exported before major processing, i.e., in the form of logs,
25 sawn timber, or manufactured wood products (Pike, 2014). Most of the CO₂ release
26 associated with harvesting will subsequently occur far away from New Zealand, e.g., in China
27 with a 34% share of New Zealand's forestry exports in 2012. In a regional inversion these
28 emissions cannot be seen (unless being transported back into the inversion domain much later,
29 as part of the background concentration), leaving a larger net sink. Emissions from harvested
30 wood products are reported in the NIR at 10.3 Tg CO₂ yr⁻¹ in 2013, translating into about 7 Tg
31 CO₂ yr⁻¹ that cannot be seen by the inversion when assuming a 70% export rate. No emissions
32 are reported for earlier years, because the harvested wood products category was introduced



1 for the first time in the 2015 report. The 2013 estimate is likely to be an upper bound for the
2 years 2011 and 2012, because the volume of harvested wood products has increased steadily
3 since 2009 (MfE, 2015). Other possible discrepancies between the NIR methodology and the
4 net CO₂ fluxes for forests include the variance in the timing of root carbon emission following
5 tree mortality (Kirschbaum et al., 2013). Large sinks observed but not accounted for in NIR
6 can result from applying steady state assumptions to natural or pre-1990 forests when they are
7 accumulating carbon in biomass during recovery from past disturbance, with potential rates of
8 biomass accumulation by native species reaching 700-900 g CO₂ m⁻² yr⁻¹ (Trotter et al., 2005).

9 For pastoral agriculture, a more complex set of differences applies to the intercomparison of
10 inversion results, *a priori* process-based model results and the NIR methodology. Similar to
11 forestry, agricultural exports (e.g. milk, meat and wool) equated to 340 g CO₂ m⁻² yr⁻¹ for a
12 dairy pasture (Mudge et al., 2011), and the 165 Gg of nitrogen estimated as exported in
13 produce (Parfitt et al., 2006) will equate to an apparent net CO₂ uptake of 5.8 Tg CO₂ yr⁻¹
14 across New Zealand. The second-most important gap between methodologies results from the
15 NIR calculation that 6.3-6.5% of the energy content of pasture consumed by ruminants is
16 converted to CH₄ emissions. These CH₄ emissions represent a carbon flux to the atmosphere
17 not observable as CO₂, and therefore require separate quantification. They have been
18 calculated as 79 g CO₂ m⁻² yr⁻¹ in a dairy pasture (Mudge et al., 2011) and the carbon content
19 of the NIR's 1137 Gg of CH₄ emissions equates to an unobserved 3.1 Tg CO₂ yr⁻¹. Several
20 additional terms, including leaching of dissolved carbon forms, and imports of feed and
21 fertiliser can also provide important corrections between net ecosystem productivity (NEP)
22 seen by inversions and eddy-covariance and net ecosystem carbon balance (NECB) (Mudge et
23 al., 2011).

24 The NIR methodology also does not account for above or below-ground grassland biomass,
25 nor does it account for soil carbon changes. The process-based model Biome-BGC potentially
26 accounts for both these flux terms, but not in relation to intensive management. Therefore,
27 both biomass and soil carbon must be considered to explain additional CO₂ uptake or loss by
28 pastures that might be seen by the inversion, but not by NIR or Biome-BGC.

29 Biomass carbon is relatively small in New Zealand pastures (Tate et al., 1997), but can be a
30 significant component of seasonal net exchange (Mudge et al., 2011; Rutledge et al., 2015;
31 Hunt et al., 2016) as described in section 7.1. Repeated measurements of soil profiles suggest
32 that soil carbon changes can also be significant but uncertain due to limited sites available for



1 resampling. A recent analysis of all sites available nationally suggests that sites on flat pasture
2 are losing soil carbon at rates of $\sim 170 \text{ g CO}_2 \text{ m}^{-2} \text{ yr}^{-1}$, while sites in hill country are gaining
3 $\sim 770 \text{ g CO}_2 \text{ m}^{-2} \text{ yr}^{-1}$ (Schipper et al., 2014). In addition to large areas of grazed pastures on
4 both islands, significant areas of tussock grasslands on the South Island could be gaining
5 biomass and soil carbon as they recover from historic overgrazing (Tate et al., 1997). The
6 extensive area of grasslands on both islands could result in large net CO_2 exchange fluxes
7 usefully observed by inversion studies. New Zealand's first process-based studies of net
8 national ecosystem carbon balance suggested large uncertainties in grasslands (Tate et al.,
9 2000) and later suggested grasslands were approximately carbon neutral in 2001 (Trotter et
10 al., 2004). Eddy covariance studies remain limited in coverage across New Zealand, but tend
11 to suggest potential for large negative NEP and near neutral NECB. Rutledge et al. (2015)
12 updated and extended the Mudge et al. (2011) results to 4 years, yielding average NEP of
13 $600 \pm 180 \text{ g CO}_2 \text{ m}^{-2} \text{ yr}^{-1}$ and NECB of $220 \pm 200 \text{ g CO}_2 \text{ m}^{-2} \text{ yr}^{-1}$. Hunt et al. (2016) also report
14 eddy-covariance carbon budgets for an irrigated intensively-grazed dairy pasture and an
15 unirrigated winter-grazed pasture in Canterbury on the South Island's east coast. Over one
16 year, the unirrigated pasture was carbon neutral ($\pm 80 \text{ g CO}_2 \text{ m}^{-2} \text{ yr}^{-1}$), while the intensively-
17 managed and irrigated pasture displayed NEP of $1500 \pm 140 \text{ g CO}_2 \text{ m}^{-2} \text{ yr}^{-1}$ and NECB of 380
18 (± 150) $\text{g CO}_2 \text{ m}^{-2} \text{ yr}^{-1}$.

19 The forest and grassland studies described above suggest that large, negative flux anomalies
20 estimated by the inversion may be plausible when extrapolated across the large areas of these
21 LCLU categories. It is important to remark that the inversion will see estimates similar to
22 NEP, but that eddy covariance studies have demonstrated that NEP can be corrected to NECB
23 using NIR-compatible data without the introduction of larger errors.

24 Additional real land carbon balance terms may also contribute to large, negative flux
25 anomalies that differ from NIR and process-based models such as Biome-BGC. These terms
26 include areas of organic soil accumulation in wet forests and bogs, typical of west-coast
27 environments where the largest negative flux anomalies are observed. Campbell et al. (2014)
28 used eddy covariance to find NEE of $800\text{--}900 \text{ g CO}_2 \text{ m}^{-2} \text{ yr}^{-1}$ with a strong seasonal cycle.
29 Erosion and deposition can also create a net carbon sink that may be unusually significant in
30 active margins such as New Zealand (Tate et al., 2000; Baisden and Manning, 2011). Small
31 catchment and site studies have estimated rates of net pasture soil carbon sequestration due to
32 erosion and burial, accounting for upland soil carbon recovery, of $220 \text{ g CO}_2 \text{ m}^{-2} \text{ yr}^{-1}$ (Page et



1 al., 2004) and $370 \text{ g CO}_2 \text{ m}^{-2} \text{ yr}^{-1}$ (Parfitt et al., 2013). Scott et al. (2006) have estimated the
2 national delivery of eroded carbon to the coast as $11 \pm 4 \text{ Tg CO}_2 \text{ yr}^{-1}$ and suggested that much
3 of this carbon is likely to be buried and replaced in uplands. Dymond (2010) attempts to more
4 fully and dynamically account for erosion, burial and replacement, suggesting a range of 4-20
5 $\text{Tg CO}_2 \text{ yr}^{-1}$. Both studies suggest the largest erosion-induced CO_2 sinks occur in the Southern
6 Alps in the west of the South Island, where the Lauder station allows observation of a strong
7 sink, as well as in the North Island's east coast. These estimates may partly be included in the
8 hill country soil carbon accumulation estimated by Schipper et al. (2014). Smith et al. (2015)
9 suggest that fiords may also create a strong carbon sink, with about 18 Mt of organic carbon
10 being buried in fjord sediments globally each year, yielding a rate of $198 \text{ g CO}_2 \text{ m}^{-2} \text{ yr}^{-1}$.
11 Thus, a number of plausible suggestions have been documented in the literature to help to
12 explain why the CO_2 sink seen by the inversion is stronger than estimated in the NIR.

13 **7.4 Uncertainty and bias assessment**

14 In addition to regional uncertainty, the posterior covariance matrix from the Bayesian
15 optimization also contains spatiotemporal error correlations between regions and every week
16 within each region. These correlations are fully taken into account when reporting
17 uncertainties for aggregated regions. Strong negative correlations between two regions would
18 indicate that the inversion is unable to distinguish their individual flux components with the
19 available data, but only their sum. Similarly, positive correlations are indicative of the
20 difference of flux components being constrained better than each individually. An analysis of
21 the error correlations reveals that both negative and positive correlations are present, however,
22 only 0.13% of all pairwise correlations have an absolute value greater than 0.1. Very few
23 values are smaller than -0.4 or greater than 0.2, with the negative extreme around -0.7 and the
24 positive extreme around 0.3. Hence, with the available data, the inversion appears able to
25 resolve weekly fluxes on the regional level chosen.

26 An analysis of the mismatch of modelled CO_2 (i.e., the CO_2 time series obtained by
27 propagating the posterior flux through the transport model) and observed CO_2 reveals
28 differences between the BHD and LAU stations (**Figure 12**). At BHD, the mismatch
29 distributions are very similar for the 13:00-14:00 and 15:00-16:00 time series, have a bias of
30 11-13% of the prior data uncertainty and show no discernible temporal pattern (smoothed,
31 thick lines in the figure). At LAU, the mismatch distribution is similar for the 13:00-14:00
32 time series, with an even smaller bias of 7%, but for the 15:00-16:00 time series there is a



1 much larger bias of 52% of the data uncertainty. This means the inversion has difficulties
2 reproducing the low CO₂ concentrations in the LAU 15:00-16:00 observational record. The
3 temporal evolution indicates an alternating pattern of small mismatch during the (austral)
4 winter and larger mismatch during summer.

5 One possible explanation is that the representation of the planetary boundary layer (PBL) in
6 the model is too shallow in the late afternoon during summer. At a site like LAU, strong solar
7 radiation during a clear summer day might lead to a sudden deepening of the PBL in the
8 afternoon between the two release periods, which might not be fully captured by the NZLAM
9 meteorology. If the real PBL is deeper than in the model, any signal from surface fluxes
10 would be mixed in a larger volume of air and measured CO₂ concentrations would be lower
11 than what is assumed by the model. The inversion would have difficulties matching these
12 lower concentrations and end up with a positive bias.

13 We compared the model boundary layer depth at 15:00-16:00 to radiosonde measurements
14 made at LAU (**Figure 13**). The Heffter method (Heffter, 1980) was used to compute PBL
15 height from the radiosonde data. The comparison suggests that the boundary layer is indeed
16 too shallow in the model during summer. However, this comparison has caveats, because the
17 radiosonde dataset is preliminary and only few measurements were taken during the right
18 time of day (15:00-16:00 LT). Furthermore, an equivalent analysis with the 13:00-14:00 LT
19 data suggests a similar discrepancy, so the question remains why these data can be explained
20 by the inversion, yet not the 15:00-16:00 LT data.

21 Results from the sensitivity scenarios (i)-(iii) are incorporated in the figures as an additional
22 uncertainty band on top of the Bayesian posterior uncertainties from the default run (**Figure**
23 **10**). That band represents the maximum (minimum) value of the flux plus (minus) its
24 uncertainty at every point in time and across all runs, i.e., including the default and sensitivity
25 runs.

26 While the uncertainty range associated with the suite of sensitivity scenarios is symmetrical
27 around the reference case for most regions, the sensitivity range is characterised by more
28 positive flux estimates than the reference case in the western South Island (**Figure 10**), i.e., a
29 slightly smaller annual carbon sink. This can be attributed to sensitivity case (iii), in which the
30 inversion is allowed to adjust air-sea fluxes to any value without penalty. Some of the
31 terrestrial CO₂ uptake is relocated to upwind ocean regions, as this yields a lower Bayesian
32 cost, because fluxes from the western South Island are shifted towards the Biome-BGC prior



1 estimates. However, in order to offset a relatively small flux change on land, the change in
2 ocean flux has to be large due to the distance to the stations and the dilution of CO₂
3 concentrations on the way. This leads to an ocean sink of 6 Pg CO₂ in 2012 in our regional
4 domain for this sensitivity test, which is more than ten times larger than estimates for the
5 whole Southern Ocean from global inversions, ocean carbon data, and ocean biogeochemistry
6 models (Gruber et al., 2009). Despite this unrealistic result for the oceans in the sensitivity
7 test, the conclusions about the seasonal pattern in CO₂ uptake and release and its spatial
8 distribution in the New Zealand land regions remain robust.

9 The inversion assumes an unbiased baseline CO₂ record. Any positive (negative) bias would
10 be interpreted by the inversion as an additional sink (source) of CO₂. From the sensitivity runs
11 we find that a constant bias in the baseline of 0.1 ppm would cause the total CO₂ flux of New
12 Zealand for each year in 2011-2013 to be off by approximately 20 Tg CO₂ yr⁻¹. This
13 corresponds to about 50% of the flux uncertainty from the default run (Table 1), thus
14 underscoring the importance of an accurate baseline in a regional inversion. Similar to the
15 sensitivity case without ocean prior, the biased baseline has only a minor influence on
16 seasonal flux patterns over land. An inversion such as ours can always benefit from advances
17 in air-sea flux datasets, such as pCO₂ measurements from a regional cruise network, as well
18 as well-characterized background air concentrations. One way to aid the baseline
19 representation in future top-down studies of the New Zealand region could be to add a
20 western component in addition to the southern and northern components, which would
21 improve the characterization of air that carries an Australian signal on top of the Southern
22 Ocean background. This could be accomplished, e.g., by establishing a CO₂ measurement
23 station situated along the west coast of South Island and choosing a western background
24 sector.

25 **8 Conclusions**

26 We present the first regional inversion estimates of air-land and air-sea CO₂ fluxes for the
27 New Zealand region, which were estimated from two *in situ* observing stations in New
28 Zealand, ship based measurements, and Lagrangian model simulations using the NAME
29 dispersion model driven by NZLAM meteorology. The results imply a strong seasonal cycle,
30 especially for fluxes in the western South Island. Regions covered predominantly by
31 indigenous forest appear to have more pronounced photosynthetic and respiratory activity



1 than suggested by the land model. This is most apparent in Fiordland, which is a key
2 contributor to the seasonal cycle, as well as the annual mean sink, in the South Island. The
3 timing, magnitude and regional distribution of seasonal flux patterns are well constrained and
4 robust across sensitivity cases, while uncertainties in annual totals are more significant.
5 Enhanced CO₂ release from the terrestrial biosphere in New Zealand is apparent in response
6 to the 2012/2013 drought period. This response appears most prominent in the North Island
7 and western parts of the South Island, consistent with reports about these regions being most
8 severely affected.

9 The annual total CO₂ sink in New Zealand is estimated to have decreased over the 3-year
10 period, at 132 ±36, 97 ±36 and 64 ±40 Tg CO₂ yr⁻¹ in 2011, 2012 and 2013, respectively. The
11 New Zealand national inventory reports a much smaller sink of 28, 27 and 27 Tg CO₂ yr⁻¹ for
12 the same years (with uncertainty around 50%). About 7 Tg CO₂ yr⁻¹ of the discrepancy can be
13 attributed to emissions associated with forest harvesting, which are included in the inventory
14 but missed by the inversion due to forestry exports. Another 13 Tg CO₂ yr⁻¹ arise from
15 different accounting of fossil emissions between the inventory and the inversion. Additional
16 factors relating to the difference between NEP and NECB in pastures can account for another
17 9 Tg CO₂ yr⁻¹. Other terms such as erosion, burial and soil carbon recovery may account for
18 another 4-20 Tg CO₂ yr⁻¹. These differences largely reconcile both results for 2013, but not
19 2011-2012. Carbon sequestration by grassland and soil carbon could also play an important
20 role in causing differences between the two methods, as these processes are not included or
21 fully resolved in inventory reporting but would be seen by the inversion. Collectively, these
22 factors are likely to reconcile both results only partially, with some differences remaining.

23 Detailed sensitivity studies suggest that the most important causes of uncertainty in the
24 inverse estimates are uncertainties in the estimate of baseline air entering the domain and air-
25 sea fluxes from the ocean surrounding New Zealand. These uncertainties could be reduced
26 through more dense pCO₂ measurements in the oceans around New Zealand, and extending
27 the ship based atmospheric CO₂ measurements presently used to estimate the baseline air
28 farther to the south and west. Another possibility is to establish additional surface stations in
29 strategic locations, i.e., with footprints in areas where Lauder and Baring Head have low
30 sensitivity, such as Rainbow Mountain in the North Island, or along the west coast of the
31 South Island.



1 The inversion methodology developed here is a powerful tool to validate net regional CO₂
2 sinks in the New Zealand national inventory report. It offers an independent, top-down view
3 on the national carbon budget.

4 **Appendix A - Lauder site description**

5 ***A.1 The Lauder station***

6 The Lauder atmospheric research station (45.038S, 169.684E, 370m AMSL) is located in the
7 broad Manuherikia river valley on the South Island of New Zealand. A semi-arid continental
8 climate predominates with an annual rainfall of 450mm and mean annual temperature of
9 9.7C. The prevailing wind is from the westerly quarter (a mean daily wind run of
10 approximately 300 km). Periodic southerly frontal systems bring air masses from the
11 Southern Ocean and Tasman Sea. The research station is located 35 km north of the township
12 of Alexandra (population: 5000). The station is surrounded by pastoral land dominated by
13 sheep and cattle farming practices along with seasonal cropping. Farming practices are non-
14 intensive and stock numbers are relatively low. The valley is sparsely populated. The land
15 westward (upwind) of the valley consists of numerous valley systems and mountainous
16 terrain. The vast majority of this land is undeveloped and is part of New Zealand's national
17 park system. There is no major industry present in the region.

18 Due to the relatively clear unclouded skies, low light pollution and low levels of local and
19 regional anthropogenic emissions, 'clean air' ground-based remote sensing, balloon sonde and
20 *in situ* measurements are routinely conducted at the station as part of NDACC (formerly
21 known as NDSC) (Kurylo, 1991), GAW (WMO-GAW, 2007), TCCON (Wunch et al., 2011)
22 and GRUAN (Seidel et al., 2009) activities.

23 ***A.2 Lauder in situ trace gas measurements***

24 Long term routine *in situ* measurements began at Lauder in 2003 with the installation of a
25 TEI-49C Ozone monitor (Zellweger et al., 2010). Previous to this only sporadic short term
26 campaigns focusing on tropospheric nitrogen dioxide had been undertaken (Johnston and
27 McKenzie, 1984). Continuous *in situ* measurements of carbon dioxide (CO₂), methane (CH₄),
28 nitrous oxide (N₂O) and carbon monoxide (CO) began in March 2007 when a prototype FTIR
29 trace gas analyser was installed (Griffith et al., 2012; Sepúlveda et al., 2014). In June 2008 a
30 well-calibrated continuous CO₂ NDIR (differential, non-dispersive, infrared) analyser (LI-



1 7000, manufactured by LI-COR, Inc, USA, www.licor.com) was installed at Lauder. This was
2 followed by regular fortnightly flask samples analysed for CO₂, CH₄, N₂O, CO and δ¹³C-CO₂
3 concentrations, starting in May 2009. An added advantage of employing the NDIR analysers
4 at both sites (Lauder and Baring Head) is that they share common data processing code and
5 calibration routines.

6 ***A.3 Air inlet system***

7 The air inlet system consists of a permanent 10 m high NIWA meteorological mast erected at
8 a distance of 33 m, to the north, from the nearest building (which also houses the *in situ*
9 instrumentation). The meteorological mast is constructed with metal irrigation piping. Two
10 sets of 60 m long (ID 8.8 mm) baked copper tubing were used to collect air from the mast
11 (inlets located at 6 m and 10 m) and deliver it to two distribution manifolds (one for each
12 sample line). A custom made inverted funnel with coarse mesh (0.7 mm) is used to provide
13 inlet rain and dust protection. In June 2012 the copper sampling lines were replaced with
14 stainless steel (SS) tubing (ID 8.8 mm). Sampling manifolds are inserted into the sampling
15 lines next to the instruments. A 100 mm long segment of PFA 9.5 mm tubing is inserted
16 between the sampling lines and the manifolds to electrically isolate sampling systems and
17 instrumentation from the meteorological mast. The manifolds are constructed from 25 mm SS
18 diameter tubing 200 mm in length (volume = 0.086 l). Each port consists of a 6.3 mm SS tube
19 welded perpendicular to the main body. Each port extends 15 mm into the main body and
20 terminated with a 45 degree angle cut facing the direction of flow.

21 Sample air is drawn into the two 4-port manifolds with a roughing pump (KNF Neuberger,
22 N035 AN18) at 10-15 l min⁻¹ giving an effective residence time of approximately 35 seconds
23 and an associated pressure drop of 40 mbar. The roughing pump allows sample air to be
24 drawn at a higher flow rate and allows multiple instruments to be connected to the sample
25 lines without front end pressure coupling between co-sampling instruments.

26 The LI-7000 is connected to one of the 10 m sampling line manifold ports with 6.3 mm
27 Synflex© (Registered 1300) tubing. The LI-7000 inlet system extracts sample air from the
28 manifold at a rate of 2.6 l min⁻¹. An FTIR trace gas analyser draws sample air from a 10 m
29 sampling line manifold port through a 6.3 mm PFA tube (300 mm length) at a rate of 3.5 l
30 min⁻¹ and the flask sampling system is connected to the same 10 m sampling line manifold
31 port with 3.2 mm Ledalon© (1200 Series Nylon 12 Tubing) tubing. When flask samples are



1 taken a flow rate of up to 2 l min^{-1} is used. Currently no measurements are taken on the 6 m
2 line.

3 ***A.4 LI-7000***

4 The LI-7000 is a commercially available dual cell NDIR analyser able to calculate CO_2 mole
5 fractions via measurements in the CO_2 $4.255 \mu\text{m}$ absorption band. The LI-7000 has been
6 proven to be a low maintenance robust CO_2 analyser able to meet GAW measurement criteria
7 when operated in the correct manner (WMO, 2001). A gas delivery and data acquisition
8 system designed by NIWA (Gomez, 1997) is used to automate and manage the delivery
9 sample and reference air along with calibration gas to the LI-7000. The LabView© data
10 acquisition program and hardware that is used to control gas delivery also performs data
11 management and display of real time instrument diagnostics. The Lauder gas handling and
12 data acquisition system is an earlier version of the current Baring Head continuous CO_2
13 monitoring system described in Brailsford et al. (2012). The main difference is that a LI-7000
14 is employed at Lauder whereas at Baring Head a Siemens Ultramat 3 gas analyser (M52012)
15 is used.

16 The LI-7000 draws air from the aforementioned air inlet system 10 m manifold via a
17 diaphragm pump (KNF Neuberger, KNF 86KNE, 2.6 Lmin^{-1}). A set of four Field standards,
18 with a calibration lineage to the mole fraction scale maintained by the CCL and a
19 target/archive tank are connected to a valve manifold consisting of five three-way (Parker
20 B16DK1175) valves in a daisy chain configuration, along with the dried air allowing selection
21 of either Field standards, target tank or sample air for the analyser. Gas regulators (Scott
22 Marin Inc, 1-SS30-590-DAT) and 1.6 mm SS tubing are used to connect tanks to the gas
23 delivery system. Compression fittings (Swagelok©) are employed for all connections. On the
24 outlet of the sample pump an overpressure is maintained on the inlet to a Nafion drier (Perma
25 Pure inc, MD-110-144S-4) with the excess flow vented, this removes the bulk of the water
26 content from the sample flow. The air sample then passes through a magnesium perchlorate
27 trap to ensure all gas to be measured has the same low water content before being introduced
28 to the analyser by a 100 sccm mass flow controller (McMillian, 80SD-5). One of the Field
29 standards is also used in the reference cell as a reference gas, and is controlled using a similar
30 mass flow controller (McMillian, 80SD-3) at 10 sccm. The exhaust sample and reference gas
31 are then dried again on molecular sieve trap before acting as the counter flow on the Nafion
32 drier, in this way dew points of -65 C are consistently met.



1 The data acquisition system selects the calibration gas to measure and monitors each Field
2 standard for stability to optimise the gas consumption. When a Field standard has a standard
3 deviation of less than 0.015 ppm over a minute it is defined as stable and the next gas is
4 measured. Sample air is continuously measured with 5-minute averages collated and reported.
5 Interspersed at regular half hourly intervals, individual Field standard tanks are measured.
6 Every 4-6 hours the suite of four Field standards is measured. A target/archive tank is
7 measured every 23 hours. Each week the Field standards and target tank are measured as a
8 separate aliquot multiple times. This sampling sequence is akin to the calibration protocol
9 employed by Brailsford et al. (2012) and Stephens et al. (2011). Data processing is performed
10 by Lauder LI-7000 specific scripts adapted from those used by (Stephens et al., 2011) and
11 written in the free statistical analysis software R.

12 Allan variance measurements (Allan, 1966) show the precision of the coupled LI-7000 -
13 NIWA gas delivery system as 0.004 ppm (1 sigma in five minutes). Calibration of the LI-
14 7000 is obtained by fitting a 3rd order polynomial to the measurements of the four Field
15 standards to characterise the concentration dependent nonlinear response of the instrument
16 every 4-6 hours. This calibration curve is then used to calibrate sample air measurements,
17 putting the measurements on the WMO X2007 scale. CO₂ concentrations of the Field
18 standards are constructed to evenly span the typical air sample concentration range
19 encountered, including elevated nocturnal levels (typical span of 380-450 ppm). Thirty
20 minute zero offsets are calculated using the interspersed individual Field standard
21 measurements. Instrument dependent artefacts (e.g instrument temperature and flushing
22 times) are accounted for in the processing code by calculating a linear fit of known Field
23 standard concentrations and the parameter in question.

24 The Field standards and the target tank are filled at BHD and characterised at the NIWA
25 GASLAB, Greta point, Wellington, New Zealand. The Field standard CO₂ concentrations are
26 calibrated to the WMO X2007 scale, along with $\delta^{13}\text{C-CO}_2$ (PDB-AIR3.3 scale) (Brailsford et
27 al., 2012). Field standards require changing every 12-18 months. The target tank requires
28 changing every 6-12 months as in parallel it also functions as a target tank for the FTIR trace
29 gas analyser.

30 *A.5 Meteorological sensors*

31 Meteorological sensors were installed onto the sampling mast. Wind speed is measured at
32 three heights (2.8 m, 5.8 m and 10.1 m) using Vector instruments A100LK anemometers. A



1 Vector instruments W200P wind vane mounted at a height of 10.1 m is used to record wind
2 direction. Relative humidity and temperature are measured using Vaisala Humitter 50U/50Y
3 sensors, placed at heights of 2.6 m and 9.9 m. In addition, a Vaisala PTB100 analog
4 barometer was installed adjacent to the *in situ* instruments (inside the building). All these
5 sensors are connected to a Campbell CR10X data logger and SDM-INT8 logger module. Ten-
6 minute averages of all sensor output are recorded independently of *in situ* gas measurement
7 instrumentation output.

8 **Appendix B - Baseline Analysis**

9 A CO₂ baseline is constructed as a weighted average of a southern and northern baseline,
10 which takes into account whether the modelled trajectories originated to the north or south of
11 the inversion domain for a given data point.

12 ***B.1 Southern Baseline***

13 The southern baseline represents a continuous record of steady background CO₂ mole
14 fractions during southerly wind conditions at BHD. A multi-step filter is applied to the BHD
15 record to obtain a CO₂ baseline representative of a large region over the Southern Ocean, as
16 described by Brailsford et al. (2012) and Stephens et al. (2013). In short, the filter selects
17 measurements during extended periods of southerly winds at the site, during which a
18 maximum standard deviation of 0.1 ppm is achieved. Additional meteorological conditions
19 must be fulfilled to preclude the influence of local sources and to ensure the air has not passed
20 over the South Island before arriving at BHD. The result of this filtering process is similar to
21 selecting observations from the southern cluster in Figure 7. The southern baseline based on
22 the filtering is used in this study.

23 After filtering the data for baseline conditions, a continuous baseline is constructed using the
24 seasonal time series decomposition by Loess (STL) algorithm (Cleveland et al., 1990), which
25 allows estimation of a long-term trend and interannually varying seasonal patterns. The STL
26 algorithm uses two time windows for the seasonal cycle and the trend, which are set by the
27 user and define the respective time periods over which variations in the data are considered.
28 The monthly averaged data fulfilling the baseline conditions are used as input, and the
29 algorithm is run first with a seasonal cycle window of 5 years and a trend window of 121
30 months to single out the decadal trend. This trend is then removed before a second run with a



1 trend window of 25 months to capture the interannual and seasonal patterns. Finally the
2 decadal, interannual and seasonal time series are summed and the resulting baseline
3 subsampled at the 13:00-14:00 and 15:00-16:00 LT windows.

4 ***B.2 Northern Baseline***

5 The northern baseline is based on *in situ* CO₂ observations using a NDIR analyser on board
6 the TF5, a ship of opportunity that cruised the triangle Japan/Australia/New Zealand about
7 once a month during the period 2011-2013 (Chierici et al., 2006). The cluster analysis showed
8 that during northerly events the air is usually coming from the northern Tasman Sea or the
9 subtropical waters to the north and only occasionally from the South Pacific eastward of New
10 Zealand. The layout of the TF5 cruises with legs crossing the Tasman Sea as well as
11 subtropical legs therefore offers the possibility to characterise the CO₂ concentrations in these
12 regions with monthly resolution. The TF5 dataset provides CO₂ concentrations averaged over
13 10 minute intervals along with the standard deviation of the high frequency measurements
14 within these intervals.

15 We defined a regional mask (**Figure 5**) to keep observations from the open ocean and avoid
16 observations taken close to the land, especially near the Australian east coast as it is located
17 upwind during average south-westerly conditions and hosts large urban centres with
18 significant CO₂ emissions. The mask spans the latitudes 39 S to 24 S. The mask was then
19 further partitioned into bands spanning one degree of latitude and the data within each band
20 averaged for each month in 2011-2013. The uncertainty of the resulting monthly record is
21 taken as the quadrature sum of the standard deviation of high-frequency data points measured
22 during the ship's transit of the respective latitude band and the standard deviation of the 10
23 minute data about the monthly mean.

24 The monthly record within each latitude band was analysed using the same STL routine as for
25 the southern baseline. An overall uncertainty estimate was formed by root mean square
26 combination of the monthly uncertainty and the time series of the remainder from the STL
27 analysis. The remainder time series is the difference between the monthly record and the sum
28 of the seasonal and trend components from the STL analysis. Finally, the STL baseline for the
29 two latitude bands for 27-26 S were averaged to produce a baseline representative of the
30 northern edge of the inversion domain at 26 S.

31 ***B.3 Weighted Baseline***



1 A day-to-day baseline was constructed as a weighted superposition of the southern and
2 northern baselines, with weights depending on the proportional latitude of air origin for the
3 twice-daily measurements at BHD and LAU. The daily NAME station footprints for the
4 13:00-14:00 and 15:00-16:00 LT windows were integrated along the southern and northern
5 edges of the domain to determine the relative fraction of back-trajectories leaving the domain
6 to the south and north. These fractions are then used to weigh the two baselines and create a
7 baseline associated with each of the twice-daily data points. Uncertainties are weighed in the
8 same way.

9 For most days the 13:00-14:00 and 15:00-16:00 LT footprints are similar with regard to the
10 origin of the air, so the weighted baselines for both time windows are almost identical. For
11 both stations on a typical day the region where the air originates is either clearly in the north
12 or the south, so that the weights for the southern and northern baselines are close to zero and
13 one, or vice versa. However, middle cases can occur when the wind conditions at a site
14 rapidly changed during the one-hour period over which measurements are collected, which
15 often results in two main branches of trajectories originating in the north and south
16 respectively. In this case both baselines are weighted proportionally to reflect the mixed
17 origin of air during the one hour averaging period for the measurements. Yet other days, or
18 periods of days, are characterised by slow wind speeds, sometimes slow enough that most
19 back-trajectories end before reaching either the northern or southern edge of the domain. In
20 this case, the midpoint of the footprint is determined and its latitude used to proportionally
21 weigh the baselines. The same procedure applies for days with trajectories leaving the domain
22 predominantly to the west or the east.

23

24 **Acknowledgements**

25 The author(s) wish to acknowledge the contribution of New Zealand eScience Infrastructure
26 (NeSI) to the results of this research. New Zealand's national compute and analytics services
27 and team are supported by the NeSI and funded jointly by NeSI's collaborator institutions and
28 through the Ministry of Business, Innovation and Employment. URL <http://www.nesi.org.nz>.
29 In addition, KNS, GB, DS, and SMF would like to acknowledge NIWA core funding through
30 the Greenhouse Gases, Emissions and Carbon Cycle Science Programme. We thank our
31 colleagues from New Zealand's Ministry for the Environment (MfE), especially the LUCAS



1 team, for very fruitful meetings. None of this work could have been accomplished without the
2 station operation teams at Baring Head and Lauder. We are grateful for access to radiosonde
3 data from Lauder, and would like to thank Ben Liley for his PBL calculations. We would also
4 like to thank Paul Wennberg and his TCCON team for the generous loan of their Li-7000 that
5 is currently at Lauder. The National Center for Atmospheric Research is sponsored by the
6 National Science Foundation.

7

8

9 References

10 Allan, D. W.: Statistics of atomic frequency standards, *Proceedings of the IEEE*, 54, 221-230,
11 1966.

12 Baisden, W. T., and Manning, M. R.: Editorial: The New Zealand carbon cycle: from regional
13 budget to global cycle, *Biogeochemistry*, 104, 1-4, 10.1007/s10533-011-9579-x, 2011.

14 Baker, D., Law, R., Gurney, K., Rayner, P., Peylin, P., Denning, A., Bousquet, P., Bruhwiler,
15 L., Chen, Y. H., and Ciais, P.: TransCom 3 inversion intercomparison: Impact of transport
16 model errors on the interannual variability of regional CO₂ fluxes, 1988–2003, *Global
17 Biogeochemical Cycles*, 20, 2006.

18 Bergamaschi, P., Krol, M., Meirink, J. F., Dentener, F., Segers, A., van Aardenne, J., Monni,
19 S., Vermeulen, A. T., Schmidt, M., Ramonet, M., Yver, C., Meinhardt, F., Nisbet, E. G.,
20 Fisher, R. E., O'Doherty, S., and Dlugokencky, E. J.: Inverse modeling of European
21 CH₄ emissions 2001–2006, *Journal of Geophysical Research*, 115, 10.1029/2010jd014180,
22 2010.

23 Blunden, J., and Arndt, D. S.: *State of the Climate in 2013*, S1-S238., 2014.

24 Brailsford, G. W., Stephens, B. B., Gomez, A. J., Riedel, K., Mikaloff Fletcher, S. E., Nichol,
25 S. E., and Manning, M. R.: Long-term continuous atmospheric CO₂
26 measurements at Baring Head, New Zealand, *Atmospheric Measurement Techniques*, 5,
27 3109-3117, 10.5194/amt-5-3109-2012, 2012.

28 Campbell, D. I., Smith, J., Goodrich, J. P., Wall, A. M., and Schipper, L. A.: Year-round
29 growing conditions explains large CO₂ sink strength in a New Zealand raised peat bog,
30 *Agricultural and Forest Meteorology*, 192-193, 59-68, 10.1016/j.agrformet.2014.03.003,
31 2014.

32 Chierici, M., Fransson, A., and Nojiri, Y.: Biogeochemical processes as drivers of surface
33 fCO₂ in contrasting provinces in the subarctic North Pacific Ocean, *Global biogeochemical
34 cycles*, 20, 2006.

35 Ciais, P., Canadell, J. G., Luysaert, S., Chevallier, F., Shvidenko, A., Poussi, Z., Jonas, M.,
36 Peylin, P., King, A. W., and Schulze, E.-D.: Can we reconcile atmospheric estimates of the
37 Northern terrestrial carbon sink with land-based accounting?, *Current Opinion in
38 Environmental Sustainability*, 2, 225-230, 2010.



- 1 Cleveland, R. B., Cleveland, W. S., McRae, J. E., and Terpenning, I.: STL: A seasonal-trend
- 2 decomposition procedure based on loess, *Journal of Official Statistics*, 6, 3-73, 1990.
- 3 Davies, T., Cullen, M. J. P., Malcolm, A. J., Mawson, M. H., Staniforth, A., White, A. A., and
- 4 Wood, N.: A new dynamical core for the Met Office's global and regional modelling of the
- 5 atmosphere, *Quarterly Journal of the Royal Meteorological Society*, 131, 1759-1782, 2005.
- 6 Dymond, J. R.: Soil erosion in New Zealand is a net sink of CO₂, *Earth Surface Processes*
- 7 *and Landforms*, 35, 1763-1772, 10.1002/esp.2014, 2010.
- 8 Dymond, J. R., Shepherd, J. D., Newsome, P. F., Gapare, N., Burgess, D. W., and Watt, P.:
- 9 Remote sensing of land-use change for Kyoto Protocol reporting: the New Zealand case,
- 10 *Environmental Science & Policy*, 16, 1-8, 2012.
- 11 Enting, I. G.: *Inverse problems in atmospheric constituent transport*, 2002.
- 12 Friedlingstein, P., Meinshausen, M., Arora, V. K., Jones, C. D., Anav, A., Liddicoat, S. K.,
- 13 and Knutti, R.: Uncertainties in CMIP5 climate projections due to carbon cycle feedbacks,
- 14 *Journal of Climate*, 27, 511-526, 2014.
- 15 Gomez, A. J.: *The CO₂ remote control system at Baring Head, Aspendale, Australia.*, 1997.
- 16 Griffith, D., Deutscher, N., Caldow, C., Kettlewell, G., Riggensch, M., and Hammer, S.: A
- 17 Fourier transform infrared trace gas and isotope analyser for atmospheric applications,
- 18 *Atmospheric Measurement Techniques*, 5, 2481-2498, 2012.
- 19 Gruber, N., Gloor, M., Mikaloff Fletcher, S. E., Doney, S. C., Dutkiewicz, S., Follows, M. J.,
- 20 Gerber, M., Jacobson, A. R., Joos, F., and Lindsay, K.: Oceanic sources, sinks, and transport
- 21 of atmospheric CO₂, *Global Biogeochemical Cycles*, 23, 2009.
- 22 Gurney, K. R., Law, R. M., Denning, A. S., Rayner, P. J., Pak, B. C., Baker, D., Bousquet, P.,
- 23 Bruhwiler, L., Chen, Y. H., and Ciais, P.: Transcom 3 inversion intercomparison: Model
- 24 mean results for the estimation of seasonal carbon sources and sinks, *Global Biogeochemical*
- 25 *Cycles*, 18, 2004.
- 26 Heffter, J.: Transport layer depth calculations, paper presented at Second Joint Conference on
- 27 Applications of Air Pollution Meteorology, Am. Meteorol. Soc., New Orleans, La, 24-28,
- 28 1980.
- 29 Hendy, J., Kerr, S., and Baisden, T.: *The Land Use in Rural New Zealand Model Version 1*
- 30 *(LURNZv1): Model Description*, Available at SSRN 994697, 2007.
- 31 Ho, D. T., Law, C. S., Smith, M. J., Schlosser, P., Harvey, M., and Hill, P.: Measurements of
- 32 air-sea gas exchange at high wind speeds in the Southern Ocean: Implications for global
- 33 parameterizations, *Geophysical Research Letters*, 33, 2006.
- 34 Hunt, J. E., Laubach, J., Barthel, M., Fraser, A., and Phillips, R. L.: Carbon budgets for an
- 35 irrigated intensively-grazed dairy pasture and an irrigated winter-grazed pasture,
- 36 *Biogeosciences Discussions*, 1-38, 10.5194/bg-2016-46, 2016.
- 37 IPCC: *IPCC, 2013: climate change 2013: the physical science basis. Contribution of working*
- 38 *group I to the fifth assessment report of the intergovernmental panel on climate change*, 2013.
- 39 Johnston, P., and McKenzie, R.: Long-path absorption measurements of tropospheric NO₂ in
- 40 rural New Zealand, *Geophysical research letters*, 11, 69-72, 1984.



- 1 Jones, A., Thomson, D., Hort, M., and Devenish, B.: The UK Met Office's next-generation
2 atmospheric dispersion model, NAME III, Air Pollution Modeling and its Application XVII,
3 580-589, 2007.
- 4 Keller, E. D., Baisden, W. T., Timar, L., Mullan, B., and Clark, A.: Grassland production
5 under global change scenarios for New Zealand pastoral agriculture, Geoscientific Model
6 Development, 7, 2359-2391, 10.5194/gmd-7-2359-2014, 2014.
- 7 Kerr, S., Anastasiadis, S., Olssen, A., Power, W., Timar, L., and Zhang, W.: Spatial and
8 temporal responses to an emissions trading scheme covering agriculture and forestry:
9 simulation results from new zealand, Forests, 3, 1133-1156, 2012.
- 10 Kidson, J. W.: An automated procedure for the identification of synoptic types applied to the
11 New Zealand region, International Journal of Climatology, 14, 711-721, 1994.
- 12 Kirschbaum, M. U. F., Saggarr, S., Tate, K. R., Thakur, K. P., and Giltrap, D. L.: Quantifying
13 the climate-change consequences of shifting land use between forest and agriculture, Science
14 of The Total Environment, 465, 314-324, <http://dx.doi.org/10.1016/j.scitotenv.2013.01.026>,
15 2013.
- 16 Kurylo, M. J.: Network for the detection of stratospheric change, Orlando'91, Orlando, FL,
17 168-174, 1991.
- 18 Le Quéré, C., Andres, R. J., Boden, T., Conway, T., Houghton, R., House, J. I., Marland, G.,
19 Peters, G. P., Van der Werf, G., and Ahlström, A.: The global carbon budget 1959–2011,
20 Earth System Science Data, 5, 165-185, 2013.
- 21 Lin, J., Gerbig, C., Wofsy, S., Andrews, A., Daube, B., Davis, K., and Grainger, C.: A near-
22 field tool for simulating the upstream influence of atmospheric observations: The Stochastic
23 Time-Inverted Lagrangian Transport (STILT) model, Journal of Geophysical Research:
24 Atmospheres, 108, 2003.
- 25 Lowe, D., Guenther, P., and Keeling, C.: The concentration of atmospheric carbon dioxide at
26 Baring Head, New Zealand, Tellus, 31, 58-67, 1979.
- 27 Manning, A. J.: The challenge of estimating regional trace gas emissions from atmospheric
28 observations, Philos Trans A Math Phys Eng Sci, 369, 1943-1954, 10.1098/rsta.2010.0321,
29 2011.
- 30 Manning, A. J., O'Doherty, S., Jones, A. R., Simmonds, P. G., and Derwent, R. G.: Estimating
31 UK methane and nitrous oxide emissions from 1990 to 2007 using an inversion modeling
32 approach, Journal of Geophysical Research, 116, 10.1029/2010jd014763, 2011.
- 33 MfE: New Zealand's Greenhouse Gas Inventory 1990-2013, Ministry for the Environment
34 (MfE) - Manatu Mo Te Taiao, Wellington, New Zealand, 2015.
- 35 Mikaloff Fletcher, S. E., Gruber, N., Jacobson, A. R., Gloor, M., Doney, S. C., Dutkiewicz,
36 S., Gerber, M., Follows, M., Joos, F., and Lindsay, K.: Inverse estimates of the oceanic
37 sources and sinks of natural CO₂ and the implied oceanic carbon transport, Global
38 Biogeochemical Cycles, 21, 2007.
- 39 Morrison, N., and Webster, H.: An assessment of turbulence profiles in rural and urban
40 environments using local measurements and numerical weather prediction results, Boundary-
41 layer meteorology, 115, 223-239, 2005.
- 42 Mudge, P. L., Wallace, D. F., Rutledge, S., Campbell, D. I., Schipper, L. A., and Hosking, C.
43 L.: Carbon balance of an intensively grazed temperate pasture in two climatically: Contrasting



- 1 years, *Agriculture, Ecosystems and Environment*, 144, 271-280, 10.1016/j.agee.2011.09.003,
2 2011.
- 3 Page, M. J., Trustrum, N. A., Brackley, H., and Baisden, W. T.: Erosion-related soil carbon
4 fluxes in a pastoral steep-land catchment, New Zealand, *Agriculture Ecosystems &*
5 *Environment*, 103, 561-579, 2004.
- 6 Parfitt, R. L., Schipper, L. A., Baisden, W. T., and Elliott, A. H.: Nitrogen inputs and outputs
7 for New Zealand in 2001 at national and regional scales, *Biogeochemistry*, 80, 71-88, 2006.
- 8 Parfitt, R. L., Baisden, W. T., Ross, C. W., Rosser, B. J., Schipper, L. A., and Barry, B.:
9 Influence of erosion and deposition on carbon and nitrogen accumulation in resampled
10 steep-land soils under pasture in New Zealand, *Geoderma*, 192, 154-159,
11 10.1016/j.geoderma.2012.08.006, 2013.
- 12 Porteous, A., and Mullan, B.: The 2012-13 drought: an assessment and historical perspective,
13 Ministry for Primary Industries (MPI), [https://www.niwa.co.nz/sites/niwa.co.nz/files/2013-
14 18-The 2012-13 drought an assessment and historical perspective.pdf](https://www.niwa.co.nz/sites/niwa.co.nz/files/2013-18-The%202012-13%20drought%20an%20assessment%20and%20historical%20perspective.pdf), 2013.
- 15 Rutledge, S., Mudge, P. L., Campbell, D. I., Woodward, S. L., Goodrich, J. P., Wall, A. M.,
16 Kirschbaum, M. U. F., and Schipper, L. A.: Carbon balance of an intensively grazed
17 temperate dairy pasture over four years, *Agriculture, Ecosystems and Environment*, 206, 10-
18 20, 10.1016/j.agee.2015.03.011, 2015.
- 19 Schipper, L. A., Parfitt, R. L., Fraser, S., Littler, R. A., Baisden, W. T., and Ross, C.: Soil
20 order and grazing management effects on changes in soil C and N in New Zealand pastures,
21 *Agriculture, Ecosystems & Environment*, 184, 67-75,
22 <http://dx.doi.org/10.1016/j.agee.2013.11.012>, 2014.
- 23 Scott, D. T., Baisden, W. T., Davies-Colley, R., Gomez, B., Hicks, D. M., Page, M. J.,
24 Preston, N. J., Tate, K. R., Trustrum, N. A., and Woods, R. A.: Localized erosion affects New
25 Zealand's national C budget, *Geophysical Research Letters*, 33, L01402. doi:
26 10.1029/2005GL024644, 10.1029/2005GL024644, 2006.
- 27 Seidel, D. J., Berger, F. H., Diamond, H. J., Dykema, J., Goodrich, D., Immler, F., Murray,
28 W., Peterson, T., Sisterson, D., and Sommer, M.: Reference upper-air observations for
29 climate: Rationale, progress, and plans, *Bulletin of the American Meteorological Society*, 90,
30 361, 2009.
- 31 Sepúlveda, E., Schneider, M., Hase, F., Barthlott, S., Dubravica, D., Garcia, O., Gomez-
32 Pelaez, A., González, Y., Guerra, J., and Gisi, M.: Tropospheric CH₄ signals as observed by
33 NDACC FTIR at globally distributed sites and comparison to GAW surface in situ
34 measurements, 2014.
- 35 Shepherd, J., and Newsome, P.: Establishing new zealand's Kyoto land use and land use-
36 change and forestry 2008 map, Contract Report LC0809/133 prepared for the Ministry for the
37 Environment. Lincoln, New Zealand, Landcare Research, 2009.
- 38 Smith, R. W., Bianchi, T. S., Allison, M., Savage, C., and Galy, V.: High rates of organic
39 carbon burial in fjord sediments globally, *Nature Geoscience*, 8, 450-453, 10.1038/ngeo2421,
40 2015.
- 41 Steinkamp, K., and Gruber, N.: A joint atmosphere-ocean inversion for the estimation of
42 seasonal carbon sources and sinks, *Global Biogeochemical Cycles*, 27, 732-745, 2013.



- 1 Stephens, B., Miles, N., Richardson, S., Watt, A., and Davis, K.: Atmospheric CO₂
2 monitoring with single-cell NDIR-based analyzers, *Atmospheric Measurement Techniques*, 4,
3 2737-2748, 2011.
- 4 Stephens, B. B., Brailsford, G. W., Gomez, A. J., Riedel, K., Mikaloff Fletcher, S. E., Nichol,
5 S., and Manning, M.: Analysis of a 39-year continuous atmospheric CO₂ record
6 from Baring Head, New Zealand, *Biogeosciences*, 10, 2683-2697, 10.5194/bg-10-2683-2013,
7 2013.
- 8 Stohl, A., Seibert, P., Arduini, J., Eckhardt, S., Fraser, P., Grealley, B., Lunder, C., Maione,
9 M., Mühle, J., and O'doherty, S.: An analytical inversion method for determining regional and
10 global emissions of greenhouse gases: Sensitivity studies and application to halocarbons,
11 *Atmospheric Chemistry and Physics*, 9, 1597-1620, 2009.
- 12 Sweeney, C., Gloor, E., Jacobson, A. R., Key, R. M., McKinley, G., Sarmiento, J. L., and
13 Wanninkhof, R.: Constraining global air-sea gas exchange for CO₂ with recent bomb 14C
14 measurements, *Global Biogeochemical Cycles*, 21, 2007.
- 15 Tait, A., Henderson, R., Turner, R., and Zheng, X.: Thin plate smoothing spline interpolation
16 of daily rainfall for New Zealand using a climatological rainfall surface, *International Journal*
17 *of Climatology*, 26, 2097-2115, 2006.
- 18 Takahashi, T., Sutherland, S. C., and Kozyr, A.: Global ocean surface water partial pressure
19 of CO₂ database: measurements performed during 1968–2008 (Version 2008),
20 ORNL/CDIAC-152, NDP-088r, Carbon Dioxide Information Analysis Center, Oak Ridge
21 National Laboratory, US Dept. of Energy, Oak Ridge, Tenn., doi, 10, 2009a.
- 22 Takahashi, T., Sutherland, S. C., Wanninkhof, R., Sweeney, C., Feely, R. A., Chipman, D.
23 W., Hales, B., Friederich, G., Chavez, F., and Sabine, C.: Climatological mean and decadal
24 change in surface ocean pCO₂, and net sea-air CO₂ flux over the global oceans (vol 56, pg
25 554, 2009), *Deep Sea Research Part I: Oceanographic Research Papers*, 56, 2075-2076,
26 2009b.
- 27 Tarantola, A.: *Inverse problem theory and methods for model parameter estimation*, 2005.
- 28 Tate, K. R., Giltrap, D. J., Claydon, J. J., Newsome, P. F., Atkinson, I. A. E., Taylor, M. D.,
29 and Lee, R.: Organic carbon stocks in New Zealand's terrestrial ecosystems, *Journal Of The*
30 *Royal Society Of New Zealand*, 27, 315-335, 1997.
- 31 Tate, K. R., Scott, N. A., Parshotam, A., Brown, L., Wilde, R. H., Giltrap, D. J., Trustrum, N.
32 A., Gomez, B., and Ross, D. J.: A multi-scale analysis of a terrestrial carbon budget - Is New
33 Zealand a source or sink of carbon?, *Agriculture Ecosystems & Environment*, 82, 229-246,
34 2000.
- 35 Thornton, P., Law, B., Gholz, H. L., Clark, K. L., Falge, E., Ellsworth, D., Goldstein, A.,
36 Monson, R., Hollinger, D., and Falk, M.: Modeling and measuring the effects of disturbance
37 history and climate on carbon and water budgets in evergreen needleleaf forests, *Agricultural*
38 *and forest meteorology*, 113, 185-222, 2002.
- 39 Thornton, P. E., Running, S. W., and Hunt, E.: Biome-BGC: terrestrial ecosystem process
40 model, Version 4.1. 1, Model product. Available on-line [[http://www. daac. ornl. gov](http://www.daac.ornl.gov)] from
41 Oak Ridge National Laboratory Distributed Active Archive Center, Oak Ridge, Tennessee,
42 USA doi, 10, 2005.
- 43 Timar, L.: *Rural Land Use and Land Tenure in New Zealand*, Available at SSRN 1970100,
44 2011.



- 1 Trotter, C. M., Tate, K. R., Saggarr, S., Scott, N. A., and Sutherland, M. A.: A multi-scale
2 analysis of a national terrestrial carbon budget and the effects of land-use change, in: Global
3 environmental change in the ocean and on land, edited by: Shiyomi M, Kawahata H, Koizumi
4 H, Tsuda A, and Y, A., TERRAPUB, Tokyo, 311-341, 2004.
- 5 Trotter, C. M., Tate, K. R., Scott, N. A., Townsend, J. A., Wilde, R. H., Lambie, S. M.,
6 Marden, M., and Pinkney, E. J.: Afforestation/reforestation of New Zealand marginal pasture
7 lands by indigenous shrublands: the potential for Kyoto forest sinks, *Annals of Forest
8 Science*, *62*, 865-871, 2005.
- 9 Turner, R.: Seasonal Climate Summary, NIWA National Climate Centre,
10 <https://www.niwa.co.nz/climate/summaries/seasonal/summer-2012-13>, 2013.
- 11 Uglietti, C., Leuenberger, M., and Brunner, D.: European source and sink areas of CO₂
12 retrieved from Lagrangian transport model interpretation of combined O₂ and CO₂
13 measurements at the high alpine research station Jungfraujoch, *Atmospheric Chemistry and
14 Physics*, *11*, 8017-8036, 10.5194/acp-11-8017-2011, 2011.
- 15 Wanninkhof, R.: Relationship between wind speed and gas exchange over the ocean, *Journal
16 of Geophysical Research: Oceans*, *97*, 7373-7382, 1992.
- 17 WMO: Global Atmosphere Watch Measurements Guide, World Meteorological Organization
18 (WMO), 2001.
- 19 WMO-GAW: WMO/GAW Strategic Plan: 2008-2015 - A Contribution to the Implementation
20 of the WMO Strategic Plan: 2008-2011, World Meteorological Organization (WMO)/Global
21 Atmosphere Watch (GAW), 2007.
- 22 Wunch, D., Toon, G. C., Blavier, J.-F. L., Washenfelder, R. A., Notholt, J., Connor, B. J.,
23 Griffith, D. W., Sherlock, V., and Wennberg, P. O.: The total carbon column observing
24 network, *Philosophical Transactions of the Royal Society of London A: Mathematical,
25 Physical and Engineering Sciences*, *369*, 2087-2112, 2011.
- 26 Zellweger, C., Steinbacher, M., Buchmann, B., and Scheel, H.: System and Performance
27 Audit of Surface Ozone, Methane, Carbon Dioxide, Nitrous Oxide and Carbon Monoxide at
28 the Global GAW Station Lauder, New Zealand, March 2010, WCC-Empa Report 10/3, 2010.

29

30

31

32

33

34



1 **Figures and Tables**

2

3 *Table 1. Annual mean CO₂ flux for selected aggregated regions, in Tg CO₂ yr⁻¹. A negative sign indicates uptake*
 4 *by the land. In parantheses the a posteriori uncertainty (1σ) is shown (excluding the sensitivity cases).*

Region	2011	2012	2013
NZ Total	-132 (36)	-97 (36)	-64 (40)
North Island	18 (28)	-40 (28)	-1 (30)
North	5 (25)	-10 (25)	7 (25)
South	13 (17)	-30 (17)	-8 (19)
South Island	-149 (22)	-56 (23)	-63 (28)
East	-37 (17)	9 (18)	-10 (23)
West	-113 (17)	-65 (16)	-52 (17)
Fiordland	-68 (13)	-22 (12)	-31 (14)

5

6

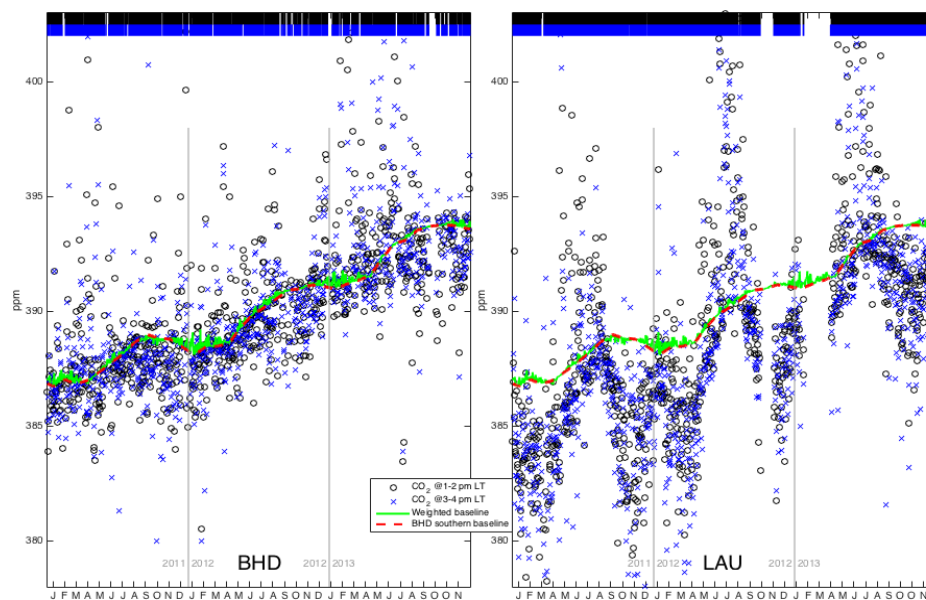


Figure 1. CO₂ observations from BHD and LAU, twice-daily at 13:00-14:00 and 15:00-16:00 LT, through 2011-13. The BHD southern baseline is shown along with the weighted baseline used in the inversion. Gaps in the coloured bars at the top indicate days when no observations are available.

7

8

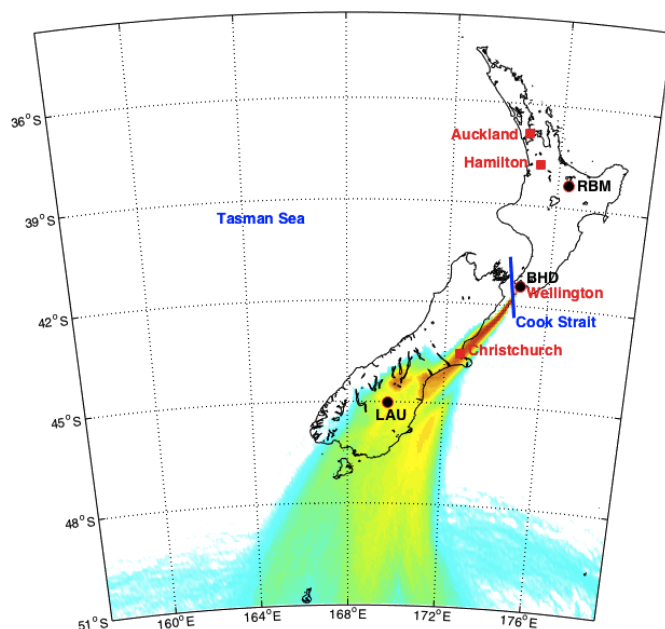


Figure 2. Air history map for 10,000 particles released at BHD during 15:00-16:00 LT on 19 May 2012 using the NAME III model. The particle back-trajectories show a southerly event locally at the station, though not a baseline event as the air crosses parts of South Island. Also shown are the locations of LAU and RBM stations.

1
2
3
4
5
6
7
8
9

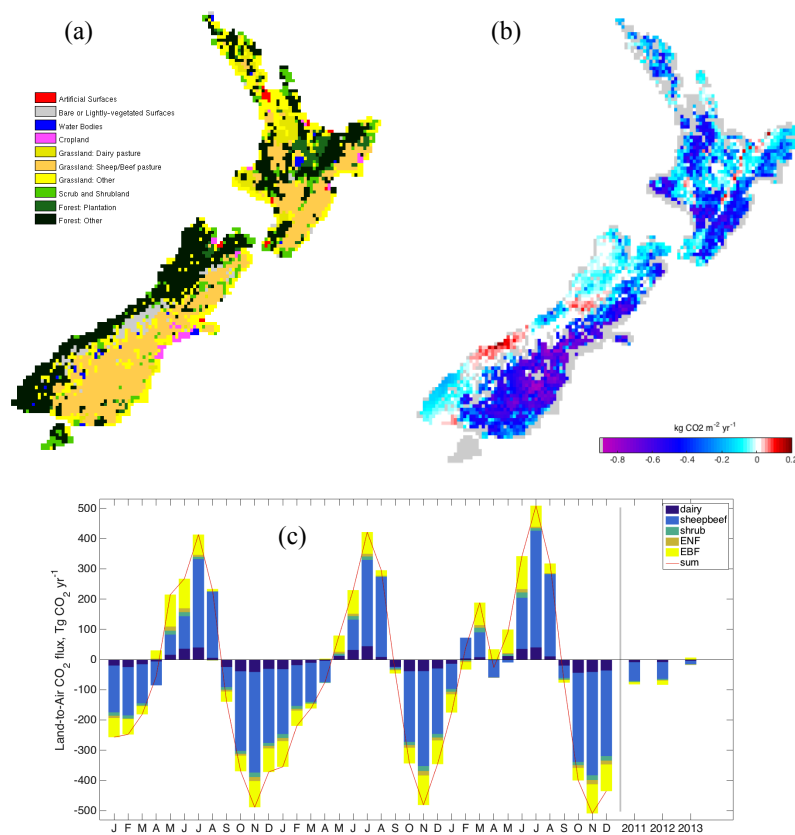


Figure 3. (a) Land-Cover/Land-Use (LCLU) map with 10 categories, based on the Land Cover Database (LCDB3) and the Land-Use in Rural New Zealand (LURNZ) basemap. (b) A priori CO₂ flux distribution, averaged over 2011-2013, from modelled NEP using BiomeBGC with the LCLU categories. Both maps have been regridded to the NAME model grid. (c) Monthly and annual contributions from each biome to the overall a priori CO₂ flux.

1
 2
 3
 4
 5
 6
 7
 8
 9

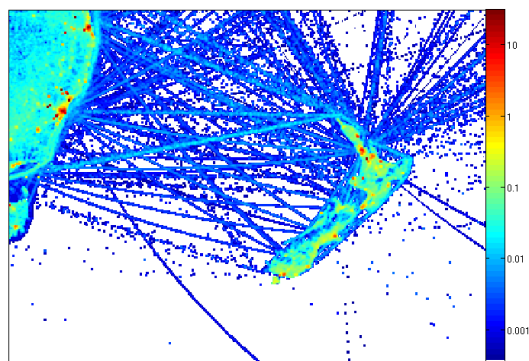


Figure 4. Gridded fossil emissions of CO₂ across the model domain and averaged over 2011-2013, in kg CO₂ m⁻² yr⁻¹. Emissions are based on EDGAR v4.2, with 2011-2013 estimates extrapolated from the 2000-2010 trend in global total emissions.

1
2
3

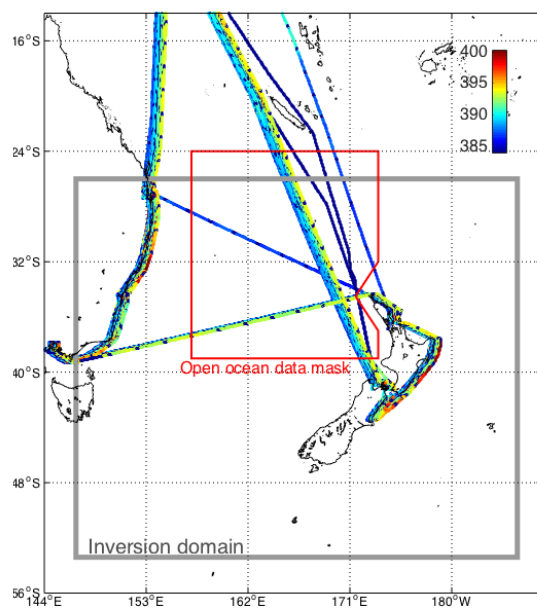


Figure 5. Voyages of the Ship of Opportunity "Trans Future 5". Ship tracks have been slightly spread longitudinally to allow one to differentiate individual cruises (more recent cruises are to the right). Colors give the in situ CO₂ concentration. Measurements made inside the open ocean mask were used in the northern baseline analysis. The inversion domain is outlined in gray.

4



1

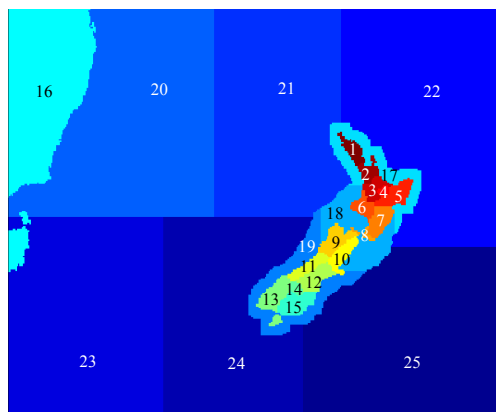


Figure 6. Regional partitioning and indices in the inversion.

2

3

4

5

6

7

8

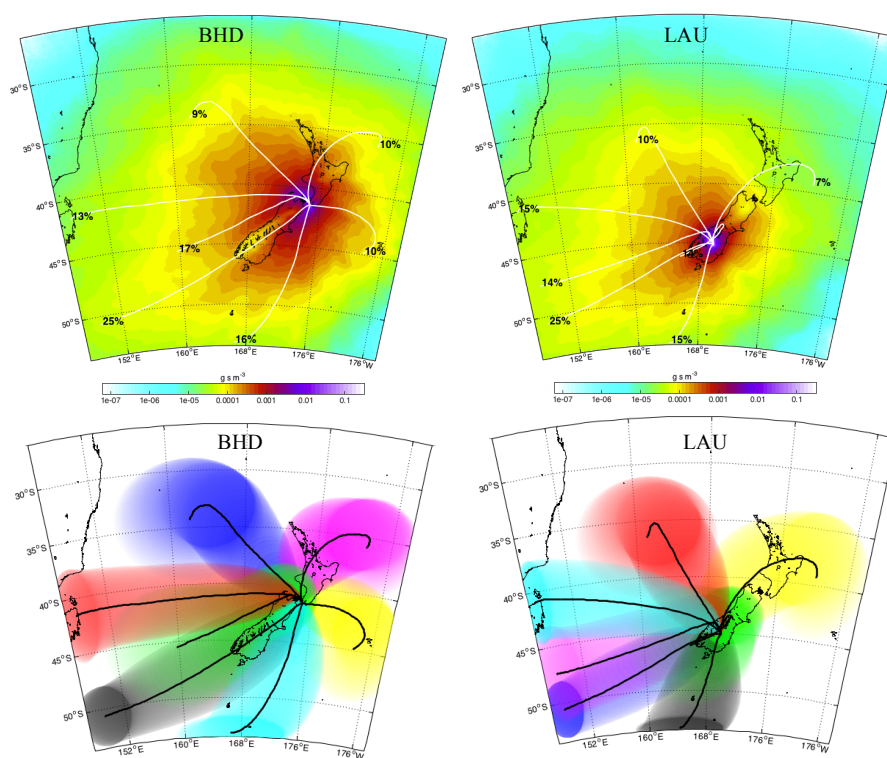


Figure 7. Top panel: 2011-2013 mean footprints for BHD and LAU stations, based on twice-daily air history maps at 13:00-14:00 and 15:00-16:00 LT. Clusters of 4-day back-trajectories are overlain. Percentages give the sizes of clusters, i.e., the probability that a particle released on a random day has followed that pathway. Lower panel: Major atmospheric transport pathways for both stations from cluster analysis of the back-trajectories from twice-daily particle release. Shades represent the geographical spread of each pathway (one standard deviation from cluster centroid in latitude/longitude).

1
2
3
4
5
6
7
8
9

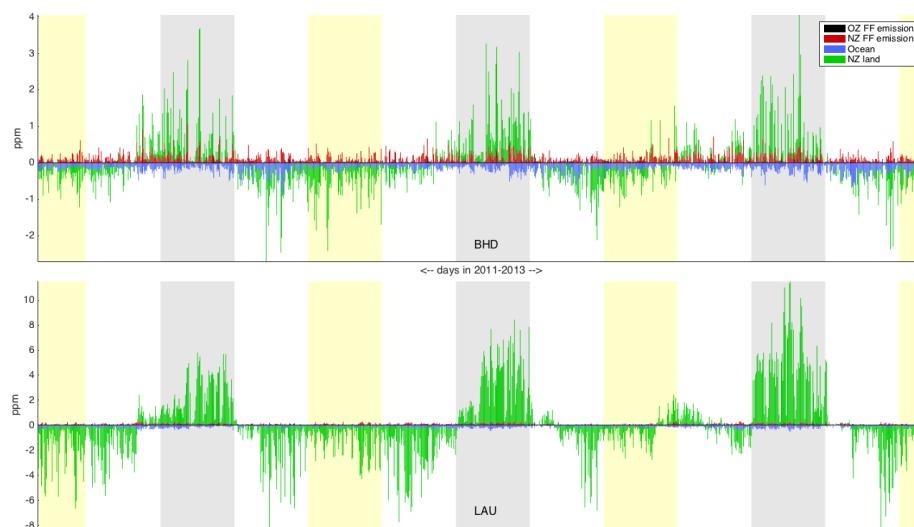


Figure 8. Simulated contributions to the observed CO_2 anomaly, i.e., concentration minus baseline, at BHD (top) and LAU (bottom) for each day in 2011-2013 averaged over both 13:00-14:00 and 15:00-16:00 LT release periods. Contributions are calculated using NAME transport matrices with EDGAR v4.2 fossil fuel emissions, prior oceanic CO_2 flux from the Takahashi $p\text{CO}_2$ dataset and prior terrestrial CO_2 flux from the BiomeBGC model. Note that scales vary due to stronger anomalies and seasonal amplitude at LAU.

1
2
3
4
5
6

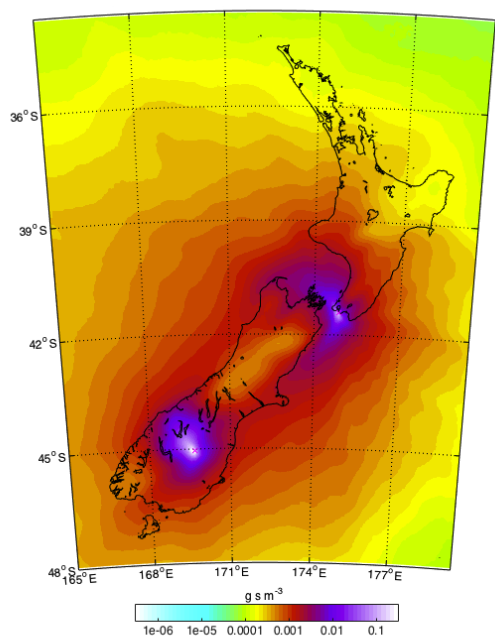


Figure 9. Combined 2011-2013 footprint for both 13:00-14:00 and 15:00-16:00 LT release periods for BHD and LAU around New Zealand.

1
2
3
4
5
6
7
8
9
10
11
12
13



1

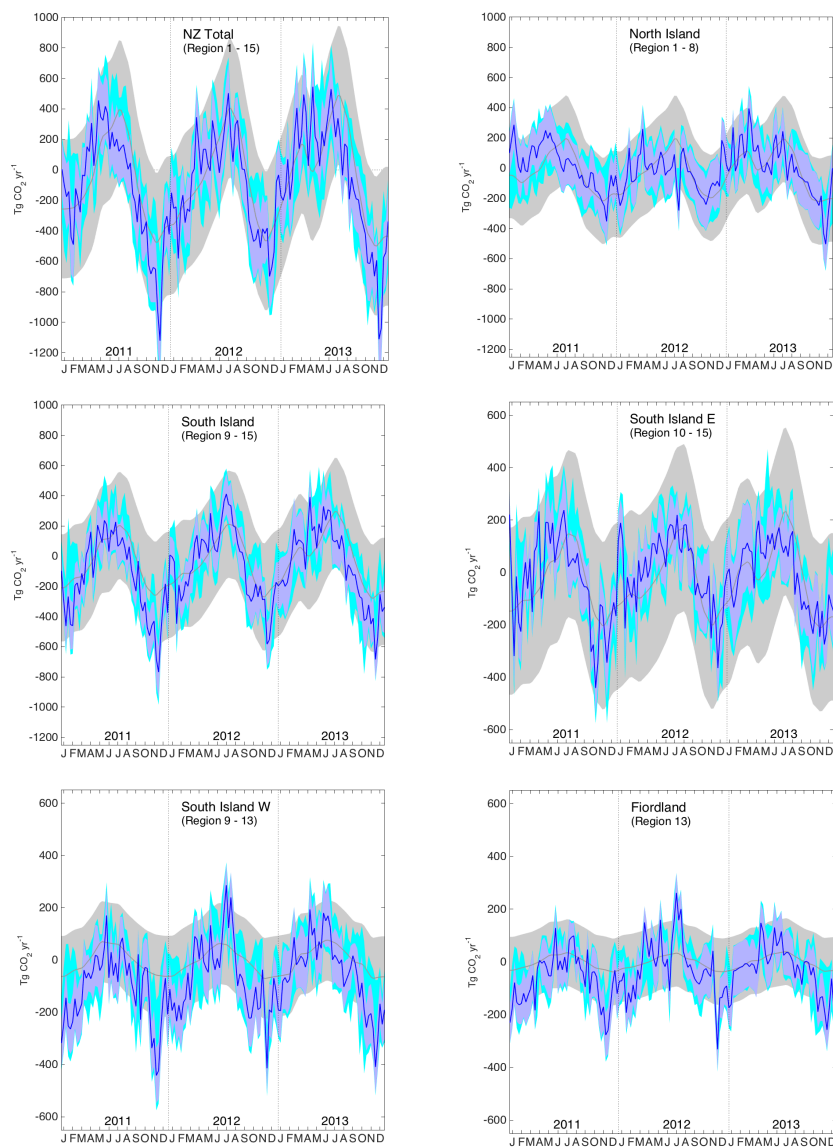


Figure 10. Weekly CO_2 fluxes in 2011–2013 from selected regions, in $\text{Tg CO}_2 \text{ yr}^{-1}$. Prior flux estimates are shown in gray and the inversion results are shown in blue. Shaded areas represent flux uncertainty (1σ). The cyan shade represents the extra uncertainty obtained from the sensitivity cases. Note there is a one-off change in scale of the flux axis for sub-island scale regions. A positive flux indicates a net release of CO_2 to the atmosphere, while a negative value indicates uptake by the land biosphere.

2

3



1
2

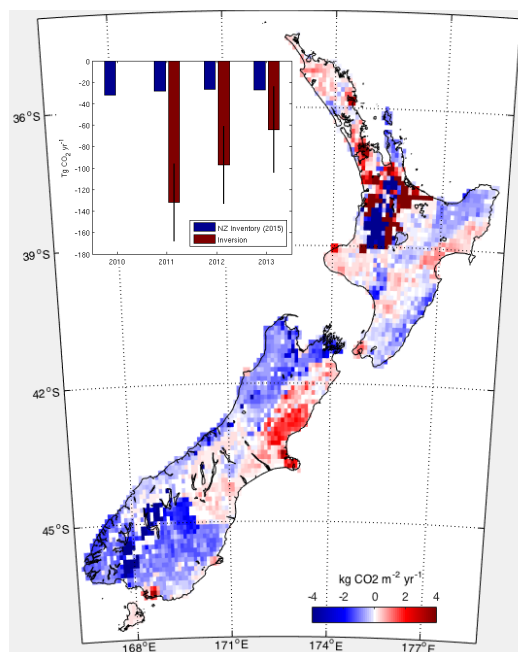


Figure 11. Geographic distribution of land-to-air CO₂ flux, averaged over 2011-2013. Blue and red regions indicate net carbon uptake and release, respectively. Per area ocean fluxes are too small to show on this scale. Fossil fuel emissions are included and reach up to 20 kg CO₂ m⁻² yr⁻¹ in a few grid cells (Auckland area). The colour scale is capped to focus on natural fluxes. Inset: Annual mean results compared to the National Greenhouse Gas Inventory Report.

3
4
5
6
7
8
9
10



1

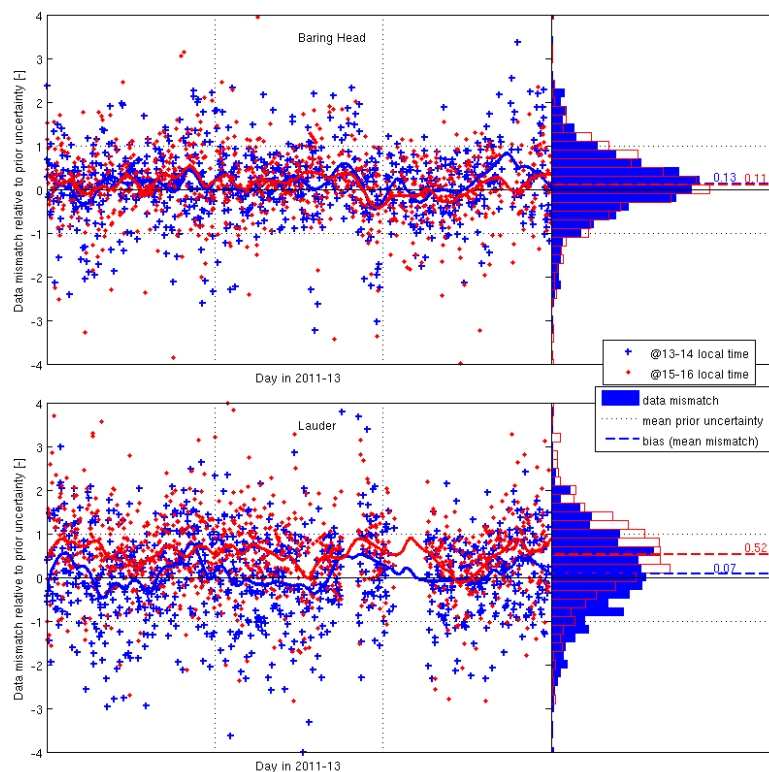


Figure 12. Mismatch (residuals) of modelled vs. observed CO_2 in multiples of the prior data uncertainty at Baring Head (top) and Lauder (bottom). Vertical dotted lines separate the years 2011, 2012 and 2013. Solid lines represent a Loess fit with a 3-month window. Horizontal dotted lines mark the prior uncertainty (1σ). The left column shows scatter plots for every day and 1 h release period; the right column shows the mismatch distribution over 2011-2013. Dashed lines with numbers give the bias.

2

3

4

5

6

7

8

9

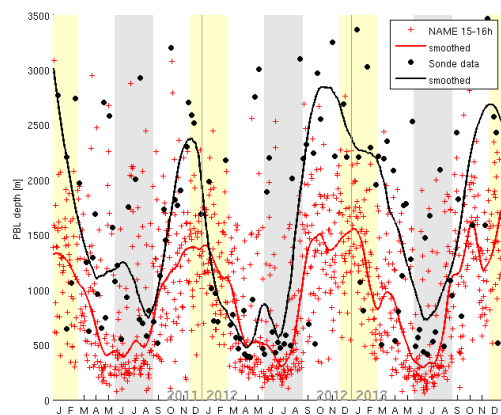


Figure 13. Comparison of boundary layer depth at LAU in NAME at 15:00-16:00 LT and radiosonde observations made at the site (Heffter method). The seasonal cycle has been made more visual using a robust Loess smoother. Summer periods are highlighted in yellow, winter periods in gray.

1

2